UTRECHT UNIVERSITY

MASTER THESIS

Intrinsic Alignment Power Spectra Predictions by use of the Anisotropic Halo Model

Author:
Theodosis PAFITIS

Supervisor:
Dr. Elisa CHISARI

A thesis submitted in fulfillment of the requirements for the degree of MSc. in Theoretical Physics

in the

Department of Physics

Utrecht University

January 21, 2023

Abstract

The halo model is an attempt to model the Universe, for the purpose of deriving analytical corrections to power spectra beyond the linear model. Previous work using the isotropic halo model, where the halos of the theory have spherical symmetry, has seen remarkable success in modelling correlations and their power spectra. Due to anisotropies emerging in the smaller scales, a generalization of the isotropic halo model has been devised, the anisotropic halo model. In this model, the halos of the theory become ellipsoidal, with different shapes and orientations. This model has been used to calculate the matter power spectrum, but it has not been used for intrinsic alignment modelling. In this project, we extend that work to intrinsic alignment modelling using the anisotropic halo model. Unlike previous work on the anisotropic model, we could not exploit several symmetries due to lack of such symmetries. We elaborate on the difficulties taking an anisotropic halo for intrinsic alignments poses, in contrast to the matter fluctuation power spectrum, and we also show our predictions. Finally, we suggest some ways to check the validity of our predictions and ways to better improve the model. We also leave some open questions regarding some results, to which we also suggest some ways one could implement to answer them.

Acknowledgements

First and foremost, I would like to express my sincerest gratitude to my supervisor Dr. Elisa Chisari, for without her continuous nurturing I would not have reached this far. She has encouraged me, inspired me and supported me, both professionally and morally. Additionally, I would like to extend my thanks to Dr. Christos Georgiou, for his invaluable assistance.

Last, but not least, I would like to thank my family and friends, for their unceasing love and support, not only during my studies but throughout every moment of my life.

Contents

Chapter 1

Introduction to Cosmology, Observations and Methods

The Universe in which we live in, is a rather complicated and interesting place, full of structure. As it is expanding at an accelerated rate, eventually all the distant galaxies and stars will vanish out of sight and go beyond the cosmological horizon. So we must appreciate living in a time where the sky is still full of observable structure, the Large-Scale Structure (LSS). Cosmology is the study of the origin and evolution of the Universe and its LSS as a whole. Cosmologists study a wide range of phenomena, including the properties and formation of galaxies and galaxy clusters, which form the LSS of the Universe, the cosmic microwave background radiation, the origins of elements heavier than hydrogen and helium and the nature of dark matter and dark energy. They use a variety of tools to study these phenomena, including mathematical modeling, computer simulations, and observations with telescopes. Cosmology is a rapidly growing and active field of research, and new discoveries are being made all the time. In the last century, we have enough evidence through observations for Einstein's theory of General Relativity to solidify as a convincing basis for a gravity model, and for Cosmology to become a precise science [1].

The Universe begins with "the Big Bang", 13.8 billion years ago from an infinitely dense and hot point; a singularity. A violent expansion then occurs, and an expanding Universe is born. As the Universe is expanding, it gradually passes through various eras, which are divided into "epochs" [2], while it cools down. The different eras are distinguished by the dominating form of energy. We start from the radiation era, which contains chaos, the hadron and the lepton epochs. Then the Universe transitions into the matter era which is when atoms form (atom epoch). Then, after the Universe's charge distribution becomes approximately zero, gravity becomes important, and all the atoms start forming overdensities of dust and gases, which collapse under their own gravity into planets and stars (stellar epoch), which then form galaxies (galaxy epoch). To this day, galaxies are still evolving and new stars keep forming. All this information can be obtained by studying the "cosmic microwave background" (CMB), which is the residual radiation of the Big Bang, which has cooled down and redshifted as the Universe kept (and keeps) expanding.

One reason behind the formation of all this structure, is due to higher density regions which cause such gravitational collapse which leads to formation of larger objects, like stars. But even after studying the CMB, the matter which we can see (baryonic matter) cannot create enough overdensities to support so much structure. Therefore, the CMB tells us that, there should be more matter in the Universe which we cannot see. We call that "dark" matter, as it does not interact with electromagnetic waves and we cannot directly observe it. It amounts to approximately 27% of the content of the Universe, while baryonic matter makes up about 5% of it. It is still unclear what the nature of this dark matter is, but its existence is well supported by the evidence, and it is the job of Cosmologists to describe what it actually is. Therefore to answer that, it is extremely useful to study all the structure we see, which we call the Large-Scale Structure (LSS), because its formation is mainly driven by dark matter.

Are we done? Not really. There are plenty of other observations which lead to make many more assumptions about the content of our Universe, and how it drives its evolution. For example, we said that the Universe is

expanding, but in what manner is it expanding? The answer is epoch dependent. In the current epoch, the Universe experiences an accelerated expansion, and the source behind this is unknown. The content of the Universe does not lead to such an expansion. It is therefore inferred that there is a form of energy, called "dark" energy, which drives the accelerated expansion of the Universe and it is currently the dominant one. There is a lot of evidence to support its existence, whether by observing the CMB or the LSS itself, but it is yet another object of which we do not understand the nature, yet. Dark energy amounts for, roughly, 68% of the content of the Universe.

To start modelling the Universe, one can clump all its content (observed and hypothetical) together and start making predictions by using General Relativity. By including dark matter and dark energy in our content, we get the most widely accepted model of our Universe, the ΛCDM model (Lambda Cold Dark Matter) which describes the evolution of the Universe in terms both of General Relativity and the Standard Model of Particle Physics. "Λ" stands for the cosmological constant in Einstein's equations, which sources accelerated expansion and therefore the constant itself accounts for the dark energy content. "Cold" dark matter refers to the velocities of the dark matter content of the Universe, which is a lot less than the speed of light, and the fact that dark matter is slow moving is supported by observation. If it were moving a lot faster, then the processes in the earlier Universe would not lead to the structure we see today. The ΛCDM model, has been successful in explaining a wide range of observations about the Universe, including the CMB, the LSS of, the observed expansion of the Universe and the abundance of light elements like Hydrogen and Helium. However, it is not without its limitations and there are some unexplained phenomena that the model cannot fully account for, such as the nature of dark matter and dark energy, as already mentioned before. Despite these limitations, the ΛCDM model remains the leading framework for understanding the evolution and structure of the Universe, and more intricate modelling can be done on its loose ends [3].

Now that we have established how important the ΛCDM is, we can now elaborate on the importance of constraining its free parameters, through observations or simulations. These parameters are crucial as they uniquely describe the content of our Universe, and its evolution. Examples consist of the density components (Ω_i, i=matter, radiation etc.), the cosmological constant and the density associated to it (Ω_Λ) and the amplitude of fluctuations in the initial conditions [1]. We will later mention exactly how these examples influence the evolution of the Universe.

The "cosmological experiment" as we call it can only be done once. We cannot repeat it! But hope is not lost. There is an abundance of data up there on the sky, and by the use of large telescopes, we can map many objects to constrain our cosmological parameters, among other goals which have already been mentioned above. Examples consist of mapping three-dimensional maps of positions of galaxies by using their redshifted light from redshift surveys (the more redshifted, the deeper they are in the sky), angular position on the sky etc. The two most famous redshift surveys are the Sloan Digital Sky Survey (SDSS) [4] and the Two Degree Field Galaxy Survey (2dF) [5]. Measurements done in the past, and current ones also confirm one very ambitious assumption of ours about the homogeneity and isotropy of the Universe; namely that over large scales the Universe actually averages to being homogeneous and isotropic! Other noteworthy surveys are the Kilo Degree Survey (KiDS) [6] and the Dark Energy Survey (DES) [7]. These surveys have dug deeper into the sky, by observing larger-redshift regions, and larger areas of the sky.

Now, exactly because the large scale average of fluctuations of fields average to zero, to start exploring the large scale structure, one often studies correlation functions of field fluctuations on the sky. For example, instead of averaging the density fluctuations over a region, we can study the correlation between densities in two different regions on our map. One probe for such a prediction could be galaxy clustering [8]. Since dark matter cannot be observed directly, it is useful to study galaxy clustering, as one can trace and try to understand dark matter by observing galaxies. Such correlations have an associated power spectrum to them, which encodes the fluctuations of the particular objects we are correlating, and can then be cross-referenced with observations from the CMB, or with simulations.

But galaxy clustering is not the only promising probe. Gravitational lensing is also as promising. From General Relativity, we know that as space-time curves, light follows along the geodesics of space-time. Thus, in the presence of dense regions that gravitate, light rays travelling from points in the sky through those regions bend. An observer then observes a sky where everything is displaced and distorted or "lensed", as shown in Figure (1.1). Galaxies appear to be at different positions on the sky, and they also appear elongated along some direction. The amount of lensing is correlated to the existence of matter or energy overdensities in the sky. Therefore, observing and measuring the amount of lensing can be thought of as gathering data on dark matter and dark energy. An immediate problem observers face is that, a deformed galaxy does not have to be intrinsically circular. Namely, a galaxy can have an ***intrinsic ellipticity*** as shown in Figure (1.2). The observed ellipticity of the galaxy is therefore affected by a combination of its intrinsic ellipticity and the induced shear due to gravitation. We are briefly mentioning this in this part of the introduction, but we will return to this point later as it is a central concept for this project.

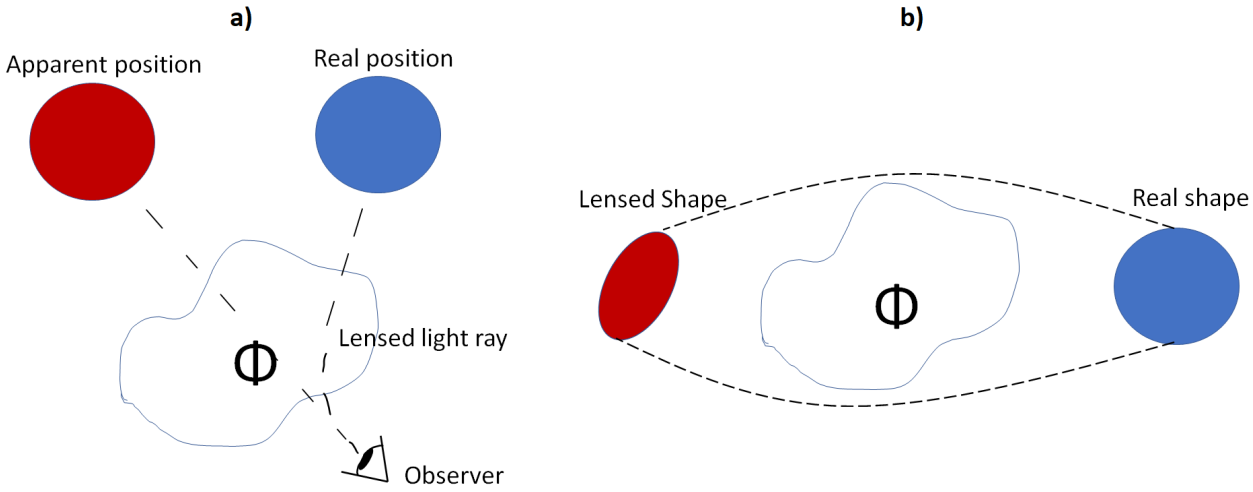

FIGURE 1.1: The picture on the left (a) shows how a light ray travelling from the blue galaxy diverges from its linear trajectory, due to a gravitational potential Φ, reaching an observer who is not directly opposite to the galaxy. The observer then sees the galaxy along the line of sight, but in reality what they see is an image, displaced from where its original resides. The picture on the right (b) shows how various lightrays beginning from a galaxy, get lensed, due to Φ, and the result is that the galaxy appears deformed and otherwise oriented as if shear forces act on it.

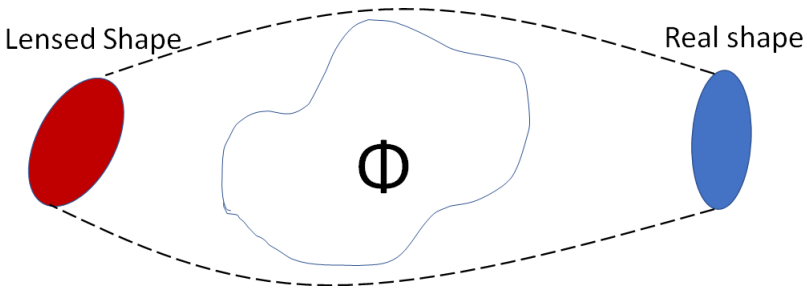

FIGURE 1.2: A galaxy can start of as elliptical (it has an intrinsic ellipticity), and appears sheared after lensing. In general it will end up looking otherwise shaped and oriented.

Another tool that greatly assists Cosmologists in studying the LSS are numerical simulations. Through N-body simulations, we have acquired a good understanding of how structure forms. Of course, the computational power is not yet enough to only simulate processes using the equations of General Relativity, so

this is mostly done using Newtonian Mechanics. Nevertheless, a good enough picture has been painted to show us that small density perturbations grow and collapse into dark matter halos, due to gravity. These halos merge into larger ones, creating a web, with the halos as the nodes and galactic filaments[1] [9] as the links between these nodes.

As a result of this observation, a model which can be used broadly has been developed called ***the halo model***. When using the halo model, we assume that all matter in the Universe lives inside halos, and their distribution is described via a density profile. Of course one needs to learn through simulations how to constrain parameters of this model, or the various distributions needed to make predictions using the model. The approach of the halo model, even if it sounds very simple, it certainly is not naive. It has provided very successful predictions regarding galaxy clustering, and has been used to also model intrinsic alignments [10].

In this work, we want to also work on obtaining various power spectra of intrinsic alignments, by using the so called ***anisotropic halo model***, the natural extension of the more widely used ***isotropic halo model***. We will first go through the analytical expressions one can provide using the isotropic halo model, and then we will show how to generalize to the anisotropic (triaxial) halo model based on the work of Jing & Suto [11] and Smith & Watts [12]. Then we will elaborate on the difficulties of performing this generalization when trying to write expressions for intrinsic alignments. We will provide a solution to that and then we show the analytical expressions that ought to be calculated using numerical methods. We will be using Monte Carlo with importance sampling just like [13].

1.1 The Mathematics Behind the Introduction

Instead of diving into halo models headfirst, let us first provide some mathematical formulation for everything said thus far. We will follow the exact same line of thought as in the introduction. We will first talk about the remnants of the Big Bang and how they drive the expansion of the Universe in various epochs. We will then introduce (more formally) the notion of correlation functions. Then we will spend some time explaining lensing, and various important parameters which are relevant for the work we do in this project. After this brief tour behind the scenes of Cosmology, we will have all the tools needed to start building a halo model, whether for predicting galaxy clustering statistics or intrinsic alignments.

1.1.1 The Lambda-CDM model

As mentioned in the introduction, the most widely accepted cosmological model is the ΛCDM model. It takes into account the existence of dark energy, by use of the cosmological constant Λ in Einstein's equation of General Relativity and it also takes into account the existence of (cold) dark matter. The content of the Universe and its curvature all have parameters associated to them called the density fraction of those components Ω_i. The expansion of the Universe is dictated by the Friedman equation (given that the metric describing the space-time geometry of the Universe is the FLRW metric):

$$\frac{H^2}{H_0^2} = \Omega_r a^{-4} + \Omega_m a^{-3} + \Omega_K a^{-2} + \Omega_\Lambda, \tag{1.1}$$

where H is the Hubble parameter and H_0 is its value today often referred to as the Hubble constant, but it is not actually a constant. It obviously changes with time, as eq. (1.1) dictates. It is approximately a constant over a period of time in an epoch. The Hubble parameter is equal to $\dot{a}/a$ where a is the scale factor of our Universe (found in the FLRW metric). The terms contributing in the evolution of the geometry of the Universe in eq. (1.1) from left to right are, the radiation, matter, curvature and dark energy density fractions. As mentioned before, the matter density fraction is a lot larger than observed, and that is because of the dark matter contributing in the matter content of our Universe.

[1] Thread-like formations

We understand now, that the evolution of our Universe is dependent on its content. This is important, because if we can solve the above equation to obtain the scale factor, we can then start calculating other important physical quantities like the comoving distances; namely distances that do not change due to the expansion of the Universe. These are defined as proper distances divided by the scale factor. We can also define the comoving angular diameter distance, in terms of the curvature K and the comoving distance χ as:

$$f_K(\chi) = \begin{cases} \frac{1}{\sqrt{K}}\sin(\sqrt{K}\chi), & K > 0 \\ \chi, & K = 0 \\ \frac{1}{\sqrt{-K}}\sinh(\sqrt{-K}\chi), & K < 0 \end{cases}$$

This will come up a bit later, when we start considering lensing and we want to calculate gravitational shear or angular correlation functions and their power spectra.

One more important thing we need for calculating lensing related effects, is the gravitational potential that causes them. By only considering linear perturbations in the theory, the gravitational potential is just a scalar Φ satisfying the Poisson equation. Taking into account the FLRW metric gives:

$$\begin{aligned} \nabla^2\Phi &= 4\pi G a^2 \widetilde{\rho}(a)\delta(\vec{r},a) \\ \delta(\vec{r},a) &= \frac{\rho(\vec{r},a)}{\widetilde{\rho}(a)} - 1 \end{aligned} \tag{1.2}$$

where δ is a fluctuation around the average matter density $\widetilde{\rho}(a)$.

By looking at eq. (1.1), one can now understand why the Universe transitions into phases which are dominated by one of its components. In the early Universe, when the scale factor is small, the radiation component is the dominant component and it mostly dictates how the Universe evolves. After the Universe has expanded enough, matter becomes more important than radiation and starts dominating. The Universe keeps expanding but at a decelerated manner. Then there is a tipping point where the Universe's expansion is accelerated, and that is why a term like Ω_Λ should be there to account for that observation. We say that we are in a dark energy dominated period.

While the Universe expands and cools down, various processes take place that end up to looking like all the magnificent structure we observe today. A cosmic web with matter halos, filaments and galaxy clusters. But how can someone study this structure? We already mentioned that there are two versatile tools. Sky surveys; studying the CMB gives details about the nature of our Universe e.g its curvature or its initial conditions, and simulations, which is the only way to study non-linear effects, especially in smaller scales. But over large scales, it suffices to do things linearly, and start building up more complex predictions about the non-linear regions. But we can only do this in a statistical manner, and that is why we have to talk about correlation functions.

1.1.2 Correlation Functions

As mentioned above, the Universe appears to be isotropic over a large scale. This means that averaging over fluctuations of observables will always lead to the trivial answer, zero. So for example, if one were interested in the matter fluctuations at one point in the sky, and averaged over a large scale, they would get:

$$\left\langle \delta(\vec{r}) \right\rangle = 0. \tag{1.3}$$

If one hopes to encode the initial conditions of the Universe inside their expressions, they would have to do it in a statistical manner [14], and the simplest non-trivial statistical object is the two-point correlation

function. For example, we can pick the matter fluctuations at two points in the sky and find their correlation (hence the name two-point correlation function):

$$\xi(\vec{r}-\vec{r}') = \left\langle \delta(\vec{r})\delta(\vec{r}') \right\rangle \tag{1.4}$$

The above quantity is often not equal to zero, which indicates that the two positions are somehow correlated due to initial conditions (which are unknown to us). Even after the Universe has expanded enough for the distance between the two to become so large that they should not have been in causal contact, they will still be correlated. This is evident from the correlations of the temperature fluctuations on the sky, as observed by the CMB. This is called the horizon problem, and the proposed solution is that, most probably, the early Universe underwent a period called ***the inflationary period***. During inflation, the Universe exponentially expands for a fraction of a second, and this hypothesis solves several problems in Cosmology, including the horizon problem. Two-point correlation functions are very useful, but what about higher order correlations?

If the fluctuation of a field has a Gaussian distribution, then higher order correlations have no additional information. Therefore it suffices to only check two-point correlations function to obtain an abundance of information, if not most of it. It turns out, that the Universe might have began with Gaussian initial conditions, and thus the two-point correlations of most of the fields we are trying to correlate, are intensely studied and no one goes for higher order expressions, with some exceptions. The exceptions include studies of primordial non-Gaussianities inside the CMB [15], and non-Gaussianities that with the LSS, due to gravity, which leaves anisotropic states at smaller scales (that is why the Universe is isotropic only when seen at a large scale). These anisotropies should be taken into account when modelling, to capture non-linear effects.

Another interesting quantity, closely tied to the two-point correlation function is the power spectrum. It essentially is the Fourier transformation of the two-point correlation function:

$$P(\vec{k}) = \int d^3r\, \xi(\vec{r}-\vec{r}')\, e^{i\vec{k}\cdot\vec{r}} \tag{1.5}$$

The reason the above is so useful is because, to obtain it one does not have to deal with convolution integrals that the two-point correlation function brings with it (because of the separation of two points).

One can create fluctuations of any field, just like we did for matter in eq. (1.2), and start correlating them or, equivalently, find their respective power spectrum. They will all depend on position or wavenumber, which are three-dimensional quantities, but one can also find angular correlations (as promised above we will see some of those when explaining gravitational shear) and their power spectra which will depend on an angle θ, measured from the line of sight of an observer and multipole l which is the equivalent of k in Fourier space.

1.1.3 The Linear Power Spectrum

We said before, that in order to capture the non-linear effects of the various processes in the Universe, one of the ways is to perform simulations. But we can at first try and focus on the larger scale, where things are linear and isotropic, and try to make an approximation of e.g the matter fluctuation power spectrum. We will call that the ***linear power spectrum*** $P_L(k)$. To do that, one relates the power spectrum of matter, to the Poisson equation in eq. (1.2) which is of linear order. The functional expression is given by [1], and it connects the (inflationary) initial conditions to the LSS, as we wanted.

If we plot the linear power spectrum (blue) and the non-linear power spectrum (red), obtained by simulations, on the same graph, as in Figure (1.3, we can see that they are the same at small wavenumbers (large scales in position space). That is a small victory, but more modelling should be done to correct for the under-predictions the linear power spectrum provides. This is what we are trying to achieve by using the

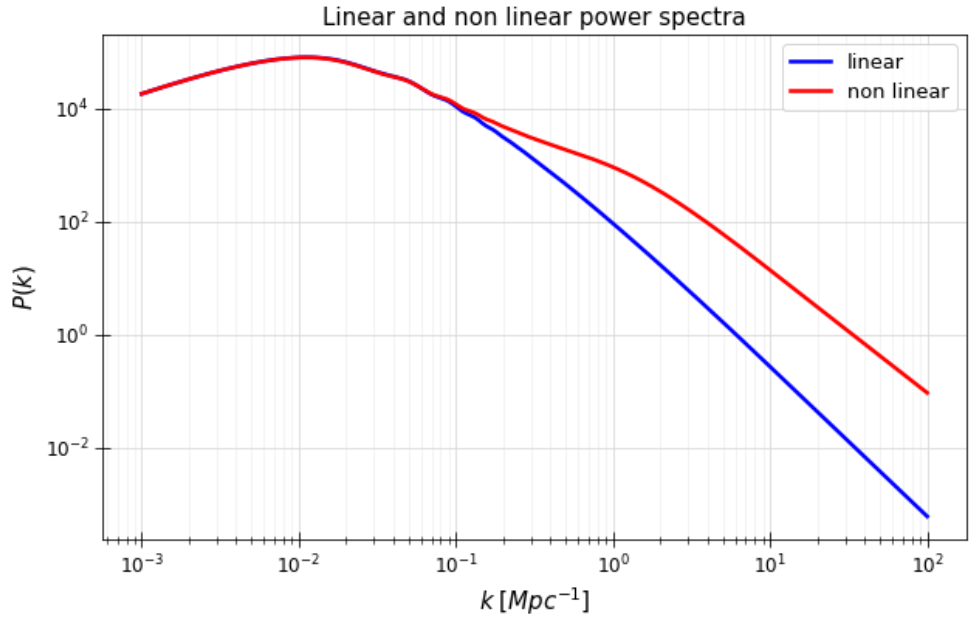

FIGURE 1.3: Linear Power Spectrum and Non-Linear Power Spectrum, taken from CCL [16].

halo model. To obtain power spectra that better predict the behavior at the mid to low scales.

Similar things will happen if we try to compare the linear power spectrum of any field with its non-linear prediction. The two will agree at large scales, but will then diverge from one another at the mid to low scales. It is our hope that by using the halo model, we will at least have better predictions than the linear model. And because this has been done in the past, quite successfully, using the isotropic halo model, it is our belief that by extending this to the anisotropic halo model (which has also been partially done in the past), we will better capture the underlying truth. But only the results will show whether our hypothesis and implementation is correct.

1.1.4 Gravitational Shear

In the introduction, we briefly mentioned that through lensing, we can probe the LSS. Particular observables of interest consist of the observed gravitational shear and the intrinsic shear/ellipticity of galaxies. Galaxies may not be entirely circular, and therefore their intrinsic ellipticity systematically affect or contaminate data of the true cosmic shear. To better understand intrinsic ellipticity, we will need to perform intrinsic alignment modelling, to understand how galaxy shapes and orientations change under the effects of tidal fields and underlying matter distribution.

Let us first examine the distortion of a galaxy shape at first order (without taking into account intrinsic ellipticity). The distortion is tied to a matrix [3]:

$$A = \begin{bmatrix} 1-\kappa-\gamma_1 & -\gamma_2 \\ -\gamma_2 & 1-\kappa+\gamma_1 \end{bmatrix}, \tag{1.6}$$

where κ is the gravitational convergence and γ is the complex gravitational shear:

$$\gamma = \gamma_1 + i\gamma_2 = |\gamma| e^{2i\phi} \tag{1.7}$$

The gravitational convergence describes the focusing of the image while the shear describes the distortions. The phase of the shear describes the orientation of the image. Gravitational shear can be written in terms of the comoving distance, as an integral along the line of sight:

$$\gamma(\theta_x,\theta_y)=\int_0^{\chi_H}d\chi\, p(\chi)\int_\chi^{\chi_H}d\chi'\frac{f_K(\chi'-\chi)f_K(\chi')}{f_K(\chi)}[\partial_y^2-\partial_x^2+2i\partial_x\partial_y]\Phi(x,y,\chi), \tag{1.8}$$

where Φ is the gravitational potential along the path from the source image to the observer, (θ_x,θ_y) are angular positions in the sky, f_K is the comoving angular distance introduced in the ΛCDM model χ_H is the comoving horizon distance and $p(\chi)$ is the probability distribution of source galaxies. Notice how the shear becomes zero, if there is no gravitational potential along the path light travels from the source to the observer. This is expected since there would not be another source for lensing besides gravitational sources. It is worth noting that this is a first order approximation, and therefore this is only useful when the lensing effects are weak, and therefore $|\gamma|<<1$.

As already mentioned in the "correlation functions" section, it will be useful to take correlations between shears to study the cosmic shear. Correlations between the shear, at different angular points in the sky, will give us insight to this cosmic shear; namely how the LSS effectively lenses objects. It can then provide on its own a good tracer of the density field of matter.

If for example one takes the correlation between shears, or even better its Fourier analogue, the angular power spectrum $C_{\gamma\gamma}(l)$, which depends on the multipole l, one can, through the Limber approximation and eq. (1.8) derive an expression in terms of the matter power spectrum:

$$C_{\gamma\gamma}(l)=\int_0^{\chi_H}d\chi\frac{q^2(\chi)}{f_K^2(\chi)}P_{\delta\delta}\left(\frac{l}{f_K(\chi)},\chi\right) \tag{1.9}$$

where $q(\chi)$ is the lensing efficiency.

But that is not the final answer for the power spectrum of the shear. As we have already mentioned, the observed shear will be systematically affected by the intrinsic ellipticity of the galaxies as well. Therefore, let us now take into account intrinsic ellipticity as well. The observed ellipticity of a galaxy is a slightly complicated function of its intrinsic ellipticity and shear due to lensing. But at first order, since we are interested in weak lensing, it can be shown that it is approximately equal to the sum of the two:

$$\varepsilon_{obs}\approx\varepsilon^I+\gamma, \tag{1.10}$$

where the superscript I denotes intrinsic. Now, we will consider correlations between observed ellipticities and intrinsic ellipticities, just like we did with the cosmic shear. In fact, we needed to show eq. (1.9) because it will be part of the total observed ellipticity power spectrum. But first, let us decompose the intrinsic ellipticity into two parts; intrinsic shear γ^I and a random part γ_{rand} which serves as noise. Then the observed shear γ_{obs} will be the difference between the observed ellipticity and the random part:

$$\gamma_{obs}=\gamma+\gamma^I \tag{1.11}$$

If the galaxies were perfectly circular, the observed shear would be the cosmic shear itself. But as we can see, the intrinsic shear of galaxies affects the observed quantity. The correlation between observed shears then becomes:

$$\left\langle\gamma_{obs}\gamma_{obs}\right\rangle=\left\langle\gamma^I\gamma^I\right\rangle+\left\langle\gamma\gamma\right\rangle+\left\langle\gamma^I\gamma\right\rangle+\left\langle\gamma\gamma^I\right\rangle, \tag{1.12}$$

and the associated angular power spectrum will be:

$$C_{\gamma_{obs}\gamma_{obs}}(l)=C_{\gamma\gamma}+C_{\gamma^I\gamma^I}(l)+C_{\gamma\gamma^I}(l) \tag{1.13}$$

where the last term in eq. (1.13) is the angular power spectrum associated to the sum of the last two terms in eq. (1.12). Let us explain the angular power spectra contributions in eq. (1.13). The first term is the cosmic shear power spectrum we derived in eq. (1.9) in terms of the density power spectrum. The second term is the intrinsic-intrinsic angular power spectrum (we will adopt the notation $C_{II}(l)$ for simplicity) and can equivalently be written in terms of the three-dimensional intrinsic-intrinsic power spectrum:

$$C_{II}(l) = \int_0^{\chi_H} d\chi \frac{p^2(\chi)}{f_K^2(\chi)} P_{II}\left(\frac{l}{f_K(\chi)}, \chi\right). \tag{1.14}$$

The third term is the angular power spectrum of the cross correlation of intrinsic shear and cosmic shear (we will adopt the notation $C_{\delta I}(l)$ for simplicity). It can also be written in terms of the three dimensional power spectrum of the the cross correlation of density and intrinsic shear, since the cosmic shear is connected to the density as seen in eqs. (1.8) & (1.9):

$$C_{\delta I}(l) = \int_0^{\chi_H} d\chi \frac{p(\chi)q(\chi)}{f_K^2(\chi)} P_{\delta I}\left(\frac{l}{f_K(\chi)}, \chi\right). \tag{1.15}$$

It is therefore evident, that in order to study the observed shear and the gravitational source (matter density) that sources it, we will have to study three-dimensional density power spectra, intrinsic shear power spectra and cross correlations between density and intrinsic shear (or better, their power spectra).

The first out of the three ingredients mentioned in the last line, has already been studied using linear approximations, and we have showed the results in Figure (1.3). We also mentioned that in order to obtain better results, one ought to perform some kind of modelling that will improve the predictions in the mid to low scales, to motivate why we are studying the halo model. Similarly, we can now show the linear approximation of the other two ingredients, the intrinsic power spectrum and density-intrinsic power spectrum, but we will again arrive at the same conclusion; namely that we will need a model to further improve the linear approximations of those two as well. That is what we strive for in the following Chapters.

For reference, the linear approximations of the δI and II power spectra, as calculated by [17], are:

$$\begin{aligned} P_{\delta I}^L(k,z) &= -A_{IA} C_1 \rho_C \frac{\Omega_m}{D(z)} P_L(k) \\ P_{II}^L(k,z) &= \left(A_{IA} C_1 \rho_C \frac{\Omega_m}{D(z)}\right)^2 P_L(k), \end{aligned} \tag{1.16}$$

where $D(z)$ is the growth factor at redshift z. We aspire to give a better picture of what is happening in the non-linear regimes, by using the halo model. For our multi-dimensional integrals, we will be using the library Vegas, like [13]. To obtain various cosmological quantities we will be using the Core Cosmology Library (CCL) [16], which has an abundance of functions to obtain useful objects like the linear and non-linear power spectra and other relevant quantities. The plots are made using Python Numpy [18].

Chapter 2

Halo Models

In this Chapter, we will focus on a model called **the halo model**, which has been useful for modelling the large-scale structure. This model has provided us with some concrete predictions for galaxy clustering and intrinsic alignments. The halo model comes in two versions; the **isotropic (spherical)** and the **anisotropic (triaxial)** one. We will first motivate the use of the halo model. Then we will discuss the formalism of the spherical version along with its results. Afterwards, we will generalize by making our model anisotropic, based on the work introduced by Smith & Watts [12]. In this thesis, we will also discuss some new theoretical predictions for intrinsic alignments, from the scope of the anisotropic halo model [19].

2.1 The Halo Model

A halo model, simply put, postulates that dark matter in the Universe, lives within halos. Of course such a claim cannot be done *a priori*. Empirical evidence is needed to pursue such a modelling path. As we already know, the Universe is mostly composed of dark matter compared to baryonic matter. Baryonic matter makes up everything that can interact with light. By observing the rotation of galaxies, one would expect that the rotational velocity, far from the center of the galaxy, would decay but instead, it flattens out! From there, we can infer the existence of unaccounted matter that can't be observed directly. The motion of gases and stars within a galaxy is not the only evidence for the existence of dark matter. Observations from gravitational lensing and N-body simulations, lead us to believe that there should be more matter, which resides in large bound regions called ***halos***. In order to model these regions, it is required to choose a shape for their boundary. The most natural choice is a sphere, by assuming isotropy, hence the name of the simplest model we will discuss, the ***isotropic halo model***. First, we will look at how can one construct this model, and what predictions does it provide. Afterwards, we will take it a step further, and construct an ***anisotropic halo model***, as a natural generalization to the isotropic version of the model. We will then discuss some theoretical predictions and how well this model fares compared to previous work.

2.1.1 Constructing the Isotropic Halo Model and Correlations of the Matter Fluctuations Field

As mentioned before, we will need to correlate several observables, or equivalently, find the respective power spectra i.e. for density fluctuations, alignments etc. As a first step, we need to identify the building blocks of such correlations. For the formulation of the halo models, both isotropic and anisotropic, we will do it in as much detail as possible by showing how to obtain the matter fluctuation correlations and power spectra. In the next Chapter we will formulate the halo model , both isotropic and anisotropic, for intrinsic alignments, but we will skip the details which are similar to this Chapter. This is because by the end of this Chapter, we will have already covered most of the basics that one should know about formulating a halo model.

Let us begin with the matter density at some point $\vec{x}$ in the Universe. We first imagine that matter is distributed inside spherical halos, described by a density profile $\rho(\vec{x}-\vec{x}_i)$, where $\vec{x}_i$ is the position of the center

of the i^{th} halo, with mass m_i. The total matter density equals the sum of the halo densities over all halos:

$$\rho(\vec{x}) = \sum_i \rho(\vec{x}-\vec{x}_i) = \sum_i m_i U(\vec{x}-\vec{x}_i|m_i), \tag{2.1}$$

where we make the common choice of using the normalized density profile:

$$\int d^3x\, U(\vec{x}|m_i) = 1. \tag{2.2}$$

It is useful to recast eq. (2.1) into integral form:

$$\begin{aligned}\rho(\vec{x}) &= \sum_i \underbrace{\left[\int d^3x' dm\, \delta^3(\vec{x}'-\vec{x}_i)\delta(m-m_i)\right]}_{\text{turning discrete variables into continuous ones}} m U(\vec{x}-\vec{x}'|m) \\ &= \underbrace{\int d^3x' dm \left[\sum_i \delta^3(\vec{x}'-\vec{x}_i)\delta(m-m_i)\right]}_{\text{changing order of integration and summation}} m U(\vec{x}-\vec{x}'|m).\end{aligned} \tag{2.3}$$

We can also define the number density of halos, usually referred to as the ***mass function*** as follows:

$$n(m) \equiv \left\langle \sum_i \delta^3(\vec{x}'-\vec{x}_i)\delta(m-m_i) \right\rangle, \tag{2.4}$$

where the quantity inside the bracket is averaged over all ensembles of realizations in a volume V:

$$\left\langle f(x) \right\rangle = \frac{1}{V}\int d^3x\, f(x). \tag{2.5}$$

The simplest computation we can consider now, is that of the mean density:

$$\begin{aligned}\widetilde{\rho} = \langle \rho(\vec{x}) \rangle &= \frac{1}{V}\int d^3x \rho(\vec{x}) \\ &= \frac{1}{V}\int d^3x \int d^3x' dm \left[\sum_i \delta^3(\vec{x}'-\vec{x}_i)\delta(m-m_i)\right] m U(\vec{x}-\vec{x}'|m) \\ &= \int dm\, m \underbrace{\frac{1}{V}\int d^3x' \left[\sum_i \delta^3(\vec{x}'-\vec{x}_i)\delta(m-m_i)\right]}_{=\mathrm{n(m)}} \underbrace{\int d^3x U(\vec{x}-\vec{x}'|m)}_{=1} \\ &= \int dm\, m\, n(m).\end{aligned} \tag{2.6}$$

The above computation, is one among many calculations that, makes use of this halo mass function from eq. (2.4). It is outside of the scope of this manuscript to explain how to obtain this function, but we will make use of the one obtained by Tinker et al [20].

We now have the basic ingredients to start considering taking correlation functions between density fluctuations at different points in space:

$$\left\langle \delta(\vec{r})\delta(\vec{r}') \right\rangle = \left\langle \left(\frac{\rho(\vec{r})}{\widetilde{\rho}} - 1\right)\left(\frac{\rho(\vec{r}')}{\widetilde{\rho}} - 1\right) \right\rangle = \frac{1}{\widetilde{\rho}^2}\langle \rho(\vec{r})\rho(\vec{r}') \rangle - 1, \tag{2.7}$$

where we use eq. (2.6) to calculate the terms linear in the density, after expanding the brackets, which

amount to a total of -2. Then by adding the remaining $+1$ we obtain a two-point correlation function and a remainder of -1. We can now plug in eq. (2.3) into eq. (2.7) to obtain:

$$\left\langle \delta(\vec{r})\delta(\vec{r}')\right\rangle = \frac{1}{\widetilde{\rho}^2}\left\langle \int d^3x' dm \left[\sum_i \delta^3(\vec{x}'-\vec{x}_i)\delta(m-m_i)\right] mU(\vec{r}-\vec{x}'|m) \right.$$
$$\left. \int d^3y' dm' \left[\sum_j \delta^3(\vec{y}'-\vec{y}_j)\delta(m'-m_j)\right] m'U(\vec{r}'-\vec{y}'|m') \right\rangle - 1. \tag{2.8}$$

We can also rearrange the operations, but other than that it is difficult to forcefully make sense of the expression in eq. (2.8). Luckily, we can naturally split it into two contributions, that are nicer to look at. Notice how we have two discrete sums over two indices i and j. Let us split the contributions of this double sum in the most obvious way possible; take the cases where i=j and $i \neq j$. Let us look at the former case first. Since the two indices are always equal, the double sum reduces to a single sum:

$$\frac{1}{\widetilde{\rho}^2}\left\langle \int d^3x' dm \int d^3y'\, dm' \left[\sum_i \delta^3(\vec{x}'-\vec{x}_i)\delta(m-m_i)\delta^3(\vec{y}'-\vec{y}_i)\delta(m'-m_i)\right] m\,m'\,U(\vec{r}-\vec{x}'|m)\,U(\vec{r}'-\vec{y}'|m')\right\rangle, \tag{2.9}$$

but the positions labeled $\vec{x}_i$ and $\vec{y}_i$, as well as the two m_i are the same. Therefore the integrals over y' and m' can be reduced, and in place of those variables, one can place either $\vec{y}_i$ and m_i or, because of the remaining two delta functions, $\vec{x}'$ and m. This leaves us with the expression:

$$\frac{1}{\widetilde{\rho}^2}\left\langle \int d^3x' dm \left[\sum_i \delta^3(\vec{x}'-\vec{x}_i)\delta(m-m_i)\right] m^2\,U(\vec{r}-\vec{x}'|m)\,U(\vec{r}'-\vec{x}'|m)\right\rangle. \tag{2.10}$$

Now all that remains is to evaluate the mean value by making use of eq. (2.5):

$$\int d^3x'\, dm\, n(m) \left(\frac{m}{\widetilde{\rho}}\right)^2 U(\vec{r}-\vec{x}'|m)\,U(\vec{r}'-\vec{x}'|m) \equiv \xi^{1h}(\vec{r}-\vec{r}'). \tag{2.11}$$

You may have noticed by now that a pattern emerges; the mass function will always appear when trying to calculate these correlation functions. That is why it was crucial to dedicate some time talking about it, even though we do not delve into the details of calculating an expression for it.

Now, we define the expression in eq. (2.11) as the ***1-halo correlation*** function ($1h$). As the name suggests, this is the contribution of one halo to the total correlation function in eq. (2.8). We must now consider the case where the indices of the sums in eq. (2.8) are always different. By following a procedure analogous to what we did from eq. (2.9) onward [1], one obtains the following expression:

$$\int d^3r_1\, dm_1\, n(m_1)\left(\frac{m_1}{\widetilde{\rho}}\right) U(\vec{r}-\vec{x}_1'|m_1) \int d^3r_2\, dm_2\, n(m_2)\left(\frac{m_2}{\widetilde{\rho}}\right) U(\vec{r}-\vec{x}_2'|m_2)\,(1+\xi_{hh}(\vec{x}_1'-\vec{x}_2'|m_1,m_2))$$
$$\hookrightarrow 1 + \int d^3r_1\, dm_1\, n(m_1)\left(\frac{m_1}{\widetilde{\rho}}\right) U(\vec{r}-\vec{x}_1'|m_1) \int d^3r_2\, dm_2\, n(m_2)\left(\frac{m_2}{\widetilde{\rho}}\right) U(\vec{r}-\vec{x}_2'|m_2)\,\xi_{hh}(\vec{x}_1'-\vec{x}_2'|m_1,m_2)$$
$$\equiv 1 + \xi^{2h}(\vec{r}-\vec{r}') \tag{2.12}$$

We do not define the above expression as the ***2-halo correlation*** function[2] ($2h$), but rather as the 2-halo correlation $+1$ for reasons which will become clear immediately.

[1] It is not exactly analogous to the 1-halo case. Taking the average is a bit more involved, and leads to the appearance of the halo-halo correlation function which does not happen trivially. We omit this discussion for simplicity.

[2] The 2-halo correlation makes use the halo-halo correlation function. This describes the clustering of halos. We will later approximate this for large scales by linear dependence on the real-space counterpart of the linear power spectrum correlation and a halo bias.

We have successfully derived two expressions, whose sum is the desired density correlation on the right hand side of eq. (2.7). By plugging in the sum of eq. (2.11) and eq. (2.12), we see that the $+1$ from eq. (2.12) cancels out nicely with the -1 in eq. (2.7), leaving us with a total correlation function as a sum of exactly two contributions; the one halo and the two halo correlation functions:

$$\left\langle \delta(\vec{r})\delta(\vec{r}\,')\right\rangle = \xi^{1h}(\vec{r}-\vec{r}\,') + \xi^{2h}(\vec{r}-\vec{r}\,') \tag{2.13}$$

It can be shown that every correlation function, not only the density fluctuations correlation (hereafter matter or density correlation), can be split into two contributions; namely $1h$ and $2h$ contributions that look similar to the integrals in eq. (2.11) and eq. (2.12). To compute such integrals, we must know the form of various functions that will always appear, like the mass function, the halo-halo correlation function and the normalized density profile. As mentioned before, we use the mass function obtained by Tinker et al. in [20].

Halo-Halo correlation and the Linear Halo Bias approximation

Regarding the halo-halo correlation, we will approximate this by using the real-space counterpart of the linear power spectrum, since it is very complicated to obtain in general. The approximation looks like this [8]:

$$\xi_{hh}(\vec{x}_1' - \vec{x}_2'|m_1,m_2) \approx b(m_1)b(m_2)\xi_L(\vec{x}_1' - \vec{x}_2'), \tag{2.14}$$

where $b(m_i)$ is the halo bias, and holds true in the large-scale regime. We will use the bias used by Tinker et al. [20].

The NFW density profile

Lastly, we need to find a functional form that describes matter distribution inside halos. The most commonly used functional form for that, was introduced by Navaro, Frank and White [21]. We call it ***the NFW profile***, and its form is the following:

$$\rho_{NFW}(r,M) = \frac{\rho_0}{\big(r/r_s\big)\big(1+r/r_s\big)^2}. \tag{2.15}$$

The r-coordinate denotes the radial distance from the center of the halo, r_s is the scale radius, hence the subscript s, and ρ_0 is a parameter to be fixed. The most natural choice to fix it is to integrate the density over the volume of the halo and set it equal to the total mass of the halo:

$$M = \int_0^R dr\, 4\pi\, \rho_{NFW}(r,M). \tag{2.16}$$

The upper limit of the integral, R, denotes the edge of the halo, and as a result, ρ_0 becomes dependent on that:

$$\rho_0 = \frac{M}{4\pi\, r_s(\log(1+c) - c/(1+c))}, \tag{2.17}$$

where $c = R/r_s$ is called ***the concentration parameter***. This parameter can be shown to have a deterministic relation to a given halo mass. For our calculations, we will use the relation used by Duffy et al. [22]:

$$c(M,z) = 7.85\Big(\frac{M}{M_p}\Big)^{-0.081}(1+z)^{-0.71} \tag{2.18}$$

where M_p is $2\times 10^{12}h^{-1}$ times the solar mass. The normalized NFW density profile $U(r|m)$ is taken to be equal to eq. (2.15) divided by the halo mass.

The Mass definition

We now have our definitions for the mass function, the halo-halo correlation function and the normalized density profile. One problem that needs to be addressed is that, when we define the functional form of our density, we need to remember that halos do not really have a well defined edge. Therefore, there's a freedom in defining that edge. This is usually done by using the over-density method of halo finding, where the density at the edge is taken to be $\Delta \times \widetilde{\rho}_X$, and the subscript X means either matter or critical density and Δ is the over-density parameter. Therefore, the mass of the halo is then defined by:

$$M = \frac{4\pi}{3}\Delta\widetilde{\rho}_X R_\Delta^3 \tag{2.19}$$

where R_Δ is the edge defined by the over-density method. The most common choice for the over-density parameter, which we will make use of, is $\Delta = 200$. Once we make this (or any) choice, and we pair it with the concentration-mass relation in eq. (2.18), we can now also define a scale radius r_s to plug back in the NFW profile. We now have everything needed to start making actual computations using the $1h$ and $2h$ expressions derived above.

The Power Spectrum

People often choose not to work with the expressions derived above but rather, they work with their Fourier transformation. The Fourier transformation of correlation functions are called ***power spectra***, and they are related via the following equation:

$$\left\langle \delta(\vec{k})\delta(\vec{k}')\right\rangle = (2\pi)^3\delta^{(3)}(\vec{k}-\vec{k}')P(\vec{k}). \tag{2.20}$$

The convenience that a power spectrum provides becomes apparent when one notices that the power spectrum is a function of a single k in momentum space, which in turn helps in avoiding convolution integrals such as those in the real space $1h$ and $2h$ correlations. Similarly to the real space correlation function, the total power spectrum can be split into a $1h$ and a $2h$ contribution:

$$P(\vec{k}) = P^{1h}(\vec{k}) + P^{2h}(\vec{k}), \tag{2.21}$$

where each term is the Fourier transformation of the $1h$ and $2h$ correlations:

$$\begin{aligned} P^{1h}(\vec{k}) &= \int dm\, n(m)\left(\frac{m}{\widetilde{\rho}}\right)^2 |U(\vec{k}|m)|^2, \\ P^{2h}(\vec{k}) &= \int dm_1 dm_2\, n(m_1)\left(\frac{m_1}{\widetilde{\rho}}\right)U(\vec{k}|m_1)\int dm_2\, n(m_2)\left(\frac{m_2}{\widetilde{\rho}}\right)U(\vec{k}|m_2)P_{hh}(\vec{k}|m_1,m_2) \end{aligned} \tag{2.22}$$

where $U(\vec{k}|m)$ is the Fourier transformation of the real space normalized NFW profile and P_{hh} is the power spectrum of the halo-halo correlation, which we will also approximate using the linear bias approximation:

$$P_{hh}(\vec{k}|m_1,m_2) = b(m_1)b(m_2)P_L(\vec{k}). \tag{2.23}$$

It is worth noting that, the Fourier transformation of the density profile, reduces to a function which only depends on the magnitude of $\vec{k}$. Thus, all the k-vectors above, can be replaced by the k-magnitude. This is an expected outcome, since the observation of density fluctuations does not depend on the direction of the observer's line of sight. We will see that in the case of alignments, this changes because observed alignments are dependent on the observer's coordinate angles and thus, their Fourier transformations should also become dependent on the direction of $\vec{k}$.

For the NFW profile, in the isotropic case, it turns out that $U(k|m)$ has an analytical solution, which makes

calculating the two power spectra in eq. (2.22) a lot easier. These two expressions can be computed numerically as well, quite easily.

2.1.2 Constructing the Anisotropic Halo Model and Correlations of the Matter Field

In the previous subsection, we discussed how to obtain a correlation function, and its power spectrum, by using the halo model and by also assuming isotropy; the halos are spherically shaped. We will now relax this assumption, and we will let the halos become ellipsoidal instead of spherical. This introduces the notion of anisotropic halos, that can have all sorts of axis ratios and orientations in space. This section is largely based on Smith & Watts [12] and Jing & Suto [11], and their work on triaxial halos.

To relax the assumption of isotropy, we must first let the halo have three distinct axes; a semi-minor and a semi-major, to which we will refer to as a and b, and a major axis c. This triplet can be sorted in a vector form, $\vec{a} = (a,b,c)$, that describes the ***shape*** of the halo. The effective degrees of freedom total to two. This is obvious since the shape of the halo's boundary is not arbitrary, it is ellipsoidal. Thus, the components of $\vec{a}$ satisfy one equation, which kills one degree of freedom. Therefore two remain; we will be using the axis ratios $\frac{a}{c}$ and $\frac{b}{c}$. Now that we have parameterized the shape, we can also define directions (unit vectors) along the principal axes of the halo, $\hat{e}_a$, $\hat{e}_b$ and $\hat{e}_c$. These quantify the ***orientation*** of the halo with respect to the observer. In general, a randomly oriented halo's axes will not align with those of the observer. The two frames of reference can always be linked via three Euler angles and three subsequent rotations involving the three angles. Just like the axes defined a shape, and were grouped as the components of a vector $\vec{a}$, we will also group the three Euler angles which define orientation as $\mathscr{E}$. A depiction of this paragraph is shown in the following Figure (2.1).

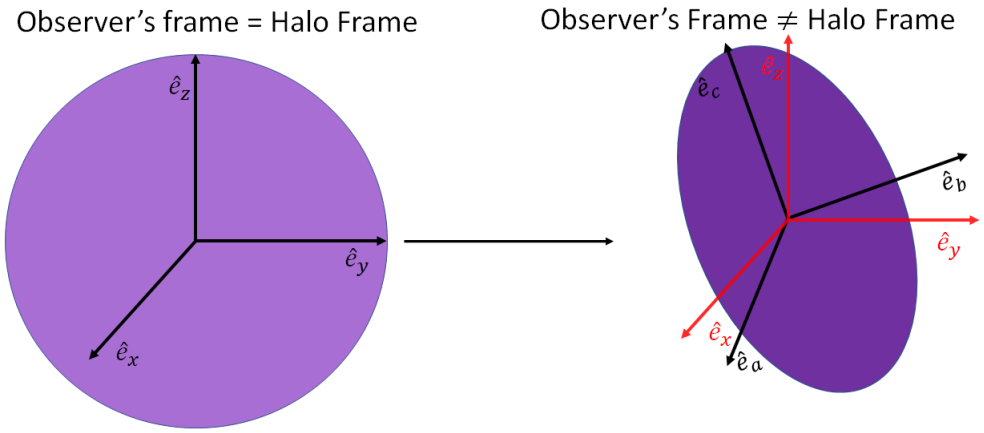

FIGURE 2.1: In the isotropic halo model, the principal axes of the halo can always be thought to be aligned with the observer's coordinate axes, due to the spherical symmetry of the halo. In the anisotropic model, the principal axes of the halo are otherwise oriented , providing a distinct orientation ($\mathscr{E}$). Also, the principal axes come in various ratios, providing a distinct shape ($\vec{a}$) to each ellipsoidal halo.

We now have anisotropic halos. We will now take the example we were using when constructing the isotropic model, the matter correlation function, and see how it looks in the anisotropic case. First of all, the density now should also become a function of shape and orientation:

$$\rho(\vec{r},M) \longrightarrow \rho(\vec{r},M,\vec{a},\mathscr{E}) = \sum_i m_i U(\vec{r}-\vec{x}_i|M_i,\vec{a},\mathscr{E}), \tag{2.24}$$

where the normalized density profile U, is now a function of shape and orientation as well. Before stating what it equals to, let us also pick a set of coordinates in which we will work with; ellipsoidal coordinates, in

the basis of the halo's frame of reference.:

$$\vec{r} = R(\frac{a}{c}\cos\Phi\sin\Theta, \frac{b}{c}\sin\Phi\sin\Theta, \cos\Theta), \tag{2.25}$$

where the parameter R, which resembles a radial coordinate, satisfies the following:

$$\frac{R^2}{c^2} = \frac{x^2}{a^2} + \frac{y^2}{b^2} + \frac{z^2}{c^2}. \tag{2.26}$$

The angles Φ and Θ play similar roles to the well known spherical ϕ and θ. They also range between $[0, 2\pi]$ and $[0, \pi]$, respectively, but we denote them with capital letters to distinguish them from the spherical ones, because they are not equal.

The Anisotropic Density Profile

In the case of the matter power spectrum, we can trivially pick a coordinate system that aligns with the principal axes of the halo because it will not matter for the matter power spectrum. This enables us to write the density profile as an NFW-like profile, but as a function of the ellipsoidal radial-like coordinate:

$$\rho(\vec{r}, M, \vec{a}, \mathscr{E}) = \rho_{NFW}(R), \tag{2.27}$$

Later, when we discuss alignments, we will explain why this choice cannot be done trivially for intrinsic alignment power spectra. In order to avoid discussing the same thing twice, we will only elaborate on this in "the Continuity Model" subsection, which is later in this Chapter.

The Anisotropic Mass Definition

Like before, we can get the mass of the halo by integrating the density over the volume. In our ellipsoidal coordinates, the integral will look like this:

$$M = 4\pi \int_0^{R_{edge}} dR R^2 \rho_{NFW}(R), \tag{2.28}$$

where R_{edge}, just like in eq. (2.19), will be chosen by the over-density method with an over-density parameter $\Delta = 200$. Namely, we pick a mass definition:

$$\begin{aligned} M &= \frac{4\pi}{3} 200 \widetilde{\rho} \frac{ab}{c^2} R_{200}^3 \\ R_{edge} &= R_{200} \end{aligned} \tag{2.29}$$

Additionally, we need to pick a convention for the Euler angles. This was not a problem before because the halos where spherical. We will use the convention used by Smith & Watts [12].

The Anisotropic Mass Function and Shape Distributions

We now have a profile, a mass definition, and an Euler angle convention. One would naively think the last ingredient to start building correlations that look like eqs. (2.11) & (2.12), is the halo mass function. Remember how integrating over mass, is equivalent to summing over all halos. In the spherical case, all halos had the same shape and orientation. Now we need to factor in that summing over all halos also means summing over all possible shapes and orientations. Which means that five more integrals are required; two for the shape, with our two axis ratios as the respective integration variables, and three for the shape, with our three Euler angles as the respective integration variables. But to do that, we need to add a distribution

for each new halo property; one shape distribution and one orientation distribution.

It turns out that we do not have to change the mass function $n(M)$ into a more complicated function. We can just multiply it by shape and orientation distributions, to obtain the substitution for the mass function:

$$n(M) \longrightarrow n(M)p_{shape}(\vec{a}|M)p_{orientation}(\mathscr{E}). \tag{2.30}$$

The subscripts *shape* and *orientation* will be omitted; it will be clear which distribution is which by its variables.

For the orientation, we expect a uniform distribution resulting in:

$$p(\mathscr{E})d\mathscr{E} = \frac{1}{2\pi}\frac{1}{2}\frac{1}{2\pi}d\alpha d(\cos\beta)d\gamma \tag{2.31}$$

where α, β, γ are the three Euler angles ranging from $[0, 2\pi]$, $[0, \pi]$ and $[0, 2\pi]$ respectively.

Regarding the shape distribution, we will use the one used by Jing & Suto [11], which separates the total probability into a conditional probability and the semi-minor's axis distribution:

$$p(\vec{a}|M) = p\big(a/b|a/c\big)p\big(a/c|M\big), \tag{2.32}$$

where the conditional probability is:

$$p\big(a/b|a/c\big) = \begin{cases} 3/(1-r_{min})\left[1-\frac{2a/b-1-r_{min}}{1-r_{min}}\right] & , \frac{a}{b} \geq r_{min} \\ 0 & , \frac{a}{b} < r_{min} \end{cases}$$

where:

$$r_{min} = \begin{cases} a/c & , \frac{a}{c} \geq 0.5 \\ 0.5 & , \frac{a}{c} < 0.5 \end{cases}$$

The axis ratio distribution is:

$$p\Big(\frac{\widetilde{a}}{c}|M\Big) = \frac{1}{\sqrt{2\pi}\sigma}\exp\left[-\frac{\left(\frac{\widetilde{a}}{c}-0.54\right)^2}{2\sigma^2}\right] \tag{2.33}$$

where $\sigma = 0.113$ and $\frac{\widetilde{a}}{c}$ is related to the mass by:

$$\frac{\widetilde{a}}{c} = \frac{a}{c}\left(\frac{M_{vir}}{M_*}\right)^{0.07[\Omega(z)]^{0.7}} \tag{2.34}$$

The M_* is called the characteristic non-linear mass at z. There is a more detailed discussion in Jing & Suto [11].

The Anisotropic Halo-Halo correlation

Now that we have a density profile, a mass definition, a mass function and our shape and orientation distributions, we are nearly ready to finally write down the anisotropic correlations of matter. There is but one small topic we ought to address. We already have everything we need to write down the $1h$ contribution. But what about the $2h$? Remember that there was one more ingredient inside that, and that was the halo-halo

correlation function. How do we deal with that in the anisotropic case?

We can still approximate it on large-scales with a linear relation to ξ_L, just like in eq. (2.14). But it will need additional pieces, that will encode information on how other halo properties are correlated, like their shape or their orientation (are those halos aligned? by how much?). These additional terms were considered by Smith & Watts [12] in an attempt to model the halo-halo correlation in the anisotropic case. But the result was that the additional terms' contribution was many orders of magnitude smaller than the original approximation. Therefore, the simpler thing for now, is to assume that shapes and alignments between halos are uncorrelated and keep the same approximations for the halo-halo correlation and power spectrum. Namely, we will keep using eq. (2.23) for our $2h$ power spectra.

The Anisotropic Power Spectra

We are finally ready to write down the anisotropic expressions for the correlation functions and power spectra. To derive these, one can follow the exact same procedure as for the isotropic case. The end result will look similar to the isotropic case. The difference is that we changed the mass definition, we added shape and orientation distributions and we are also integrating over axis ratios and orientations.

The new correlation functions will become:

$$\begin{aligned}
\xi^{1h}(\vec{r}-\vec{r}') &= \frac{1}{\widetilde{\rho}^2}\int d^3x\, dM\, d\mathscr{E}\, d\vec{a}\; n(M)\, M^2\, p(\vec{a}|M)\, p(\mathscr{E})\, U(\vec{r}-\vec{x}|M) U(\vec{r}'-\vec{x}|M) \\
\xi^{2h}(\vec{r}-\vec{r}') &= \frac{1}{\widetilde{\rho}^2}\int d^3x_1\, dM_1\, d\mathscr{E}_1\, d\vec{a}_1\; n(M_1)\, M_1\, p(\vec{a}_1|M_1)\, p(\mathscr{E}_1)\, U(\vec{r}-\vec{x}_1|M_1) \\
&\qquad \int d^3x_2\, dM_2\, d\mathscr{E}_2\, d\vec{a}_2\; n(M_2)\, M_2\, p(\vec{a}_2|M_2)\, p(\mathscr{E}_2)\, U(\vec{r}'-\vec{x}_2|M_2)\, \xi_{hh}(\vec{x}_1-\vec{x}_2|m_1,m_2)
\end{aligned} \tag{2.35}$$

and the corresponding power spectra:

$$\begin{aligned}
P^{1h}(\vec{k}) &= \frac{1}{\widetilde{\rho}^2}\int dM\, d\mathscr{E}\, d\vec{a}\; n(M)\, M^2\, p(\vec{a}|M)\, p(\mathscr{E})\, |U(\vec{k}|M)|^2 \\
P^{2h}(\vec{k}) &= \frac{1}{\widetilde{\rho}^2}\int dM_1\, d\mathscr{E}_1\, d\vec{a}_1\; n(M_1)\, M_1\, p(\vec{a}_1|M_1)\, p(\mathscr{E}_1)\, U(\vec{k}|M_1) \\
&\qquad \int dM_2\, d\mathscr{E}_2\, d\vec{a}_2\; n(M_2)\, M_2\, p(\vec{a}_2|M_2)\, p(\mathscr{E}_2)\, U^*(\vec{k}|M_2)\, P_{hh}(\vec{k}|m_1,m_2)
\end{aligned} \tag{2.36}$$

where U is the NFW-like profile in ellipsoidal coordinates. All functions inside the integrals are known, therefore all that remains is simply calculating the expressions given above. It is worth to note though, that they are quite high-dimensional integrals, and therefore it would be helpful to try and squeeze them into slightly simpler expressions.

The Continuity Model

Before simplifying our expressions, let us first talk about the density profile. We mentioned in the previous paragraph that U is the NFW-like profile in ellipsoidal coordinates. But how is this justified, when our halos are now ellipsoidal and not spherical? In Jing & Suto [11], they tried fitting an NFW-like profile, using the ellipsoidal radial coordinate R. It turns out that the NFW profile itself, in those coordinates, is good enough for the power spectra that we are considering here. This is what Smith & Watts ([12] refer to as ***the continuity model***. They deform the sphere into an ellipsoid, without changing the volume of the halo. As a result, the density becomes:

$$\rho_{cont}(R) = \frac{\rho_0}{\frac{R}{R_0}\left(1+\frac{R}{R_0}\right)^2} \tag{2.37}$$

and the edge of the halo becomes:

$$R_{edge} = \left(\frac{ab}{c^2}\right)^{-\frac{1}{3}}(R_{200}) \tag{2.38}$$

Therefore, using the concentration parameter c, and the new definition for R_{edge}, one can get $R_0 = R_{200}/c$ and plug it back to eq. (2.37) to obtain a density profile.

Computing the Anisotropic Power Spectra

Now that everything has been defined, we can start plugging functions inside eqs. (2.35) & (2.36), and try to simplify them as much as we can, before trying to solve them numerically.

Let us first look at the $1h$ term. It is often written like this in the literature:

$$P^{1h}(\vec{k}) = \frac{1}{\bar{\rho}^2}\int dM\, d\vec{a}\, n(M)\, M^2\, p(\vec{a}|M)\, W(\vec{k}) \tag{2.39}$$

where $W(\vec{k})$ is called the window function:

$$\begin{aligned} W(\vec{k}) &= \int d\mathscr{E}\, p(\mathscr{E})\, |U(\vec{k}|M)|^2 \\ &= \int d\mathscr{E}\, p(\mathscr{E}) \left| \int d^3x\, U(\vec{x}|M) \exp\left[i\vec{k}\cdot\vec{x}\right]\right|^2 \end{aligned} \tag{2.40}$$

which equals the Fourier transformation of the continuity profile squared, integrated over all possible orientations. In Smith & Watts [12], they exploit a symmetry of the system; integrating over all orientations for a fixed $\vec{k}$ is equivalent to integrating over all directions $\hat{k}$ for a fixed orientation (this only works in the matter case). Thus the following substitution can be made:

$$\int d\mathscr{E}\, p(\mathscr{E}) \equiv \int \frac{d\hat{k}}{4\pi} \tag{2.41}$$

By choosing to work in ellipsoidal coordinates, eq. (2.40) becomes:

$$W(\vec{k}) = \int \frac{d\hat{k}}{4\pi} \left|\frac{ab}{c^2}\int dR\, R^2\, U(R|M) \int d\Theta\, \sin(\Theta) \int d\Phi\, \exp\left[-i\vec{k}\cdot\vec{x}(R,\Theta,\Phi)\right]\right|^2 \tag{2.42}$$

Let's focus on the angular integration part. We can start by explicitly performing the inner product on the exponent:

$$\begin{aligned} &\int d\Theta \sin(\Theta) d\Phi\, \exp\left[i\vec{k}\cdot\vec{x}(R,\Phi,\Theta)\right] = \\ &= \int d\Theta \sin\Theta\, \exp[ikR\cos\theta_k\cos\Theta] \int d\Phi\, \exp[ikR\frac{a}{c}\sin\theta_k\sin\Theta\cos\phi_k\cos\Phi + ikR\frac{b}{c}\sin\theta_k\sin\Theta\sin\phi_k\sin\Phi] \end{aligned} \tag{2.43}$$

where we split the part that only depends on Θ from the rest of the expression. We can now make use of the following known integral:

$$\int_0^{2\pi} d\phi\, \exp[iu\cos\phi + iv\sin\phi] = 2\pi J_0(\sqrt{u^2+v^2}) \tag{2.44}$$

to integrate over Φ in eq. (2.43):

$$\begin{aligned}&\int d\Theta \sin(\Theta) d\Phi \, \exp\left[i\vec{k}\cdot\vec{x}(R,\Phi,\Theta)\right] = \\ &= \int d\Theta \sin\Theta \, \exp[ikR\cos\theta_k\cos\Theta]\left[2\pi J_0\left(kR\sin\theta_k\sin\Theta\sqrt{\left(\frac{a}{c}\right)^2\cos^2\phi_k+\left(\frac{b}{c}\right)^2\sin^2\phi_k}\right)\right]\end{aligned} \tag{2.45}$$

Now, to solve the above integral, it is useful to write the exponential into its real and imaginary components:

$$\begin{aligned}Real &= \int d\Theta \sin\Theta \, \cos(kR\cos\theta_k\cos\Theta)\left[2\pi J_0\left(kR\sin\theta_k\sin\Theta\sqrt{\left(\frac{a}{c}\right)^2\cos^2\phi_k+\left(\frac{b}{c}\right)^2\sin^2\phi_k}\right)\right] \\ Imaginary &= \int d\Theta \sin\Theta \, \sin(kR\cos\theta_k\cos\Theta)\left[2\pi J_0\left(kR\sin\theta_k\sin\Theta\sqrt{\left(\frac{a}{c}\right)^2\cos^2\phi_k+\left(\frac{b}{c}\right)^2\sin^2\phi_k}\right)\right]\end{aligned} \tag{2.46}$$

We can now group and rename parameters in the above expressions and make a change of variable; namely we rename $kR\cos\theta_k \longrightarrow a$, $kR\sin\theta_k\sqrt{\left(\frac{a}{c}\right)^2\cos^2\phi_k+\left(\frac{b}{c}\right)^2\sin^2\phi_k} \longrightarrow b$ and we change $\cos\Theta \longrightarrow x$. The integration boundaries change from $[0,\pi]$ to $[-1,1]$:

$$\begin{aligned}Real &= \int_{-1}^{1} dx\sqrt{1-x^2}\, \cos(ax)\left[2\pi J_0\left(b\sqrt{1-x^2}\right)\right] \\ Imaginary &= \int_{-1}^{1} dx\sqrt{1-x^2}\, \sin(ax)\left[2\pi J_0\left(b\sqrt{1-x^2}\right)\right],\end{aligned} \tag{2.47}$$

Notice how $\sqrt{1-x^2}$ is symmetric around zero in the domain of integration. The real integral is completely symmetric, thus it can also be written as:

$$Real = 4\pi\int_{0}^{1} dx\sqrt{1-x^2}\, \cos(ax) J_0\left(b\sqrt{1-x^2}\right), \tag{2.48}$$

whereas, the imaginary part amounts to zero because it is antisymmetric. Therefore, only the real part of the exponential contributes in the angular integration. We use a known integral to finally obtain:

$$\begin{aligned}4\pi\int_{0}^{1} dx\sqrt{1-x^2}\, \cos(ax) J_0\left(b\sqrt{1-x^2}\right) &= 4\pi j_0(\sqrt{a^2+b^2}) \\ &= 4\pi j_0\left(kR\sqrt{\cos^2\theta_k+\sin^2\theta_k\left[\left(\frac{a}{c}\right)^2\cos^2\phi_k+\left(\frac{b}{c}\right)^2\sin^2\phi_k\right]}\right) \\ &= 4\pi j_0\Big(kRf(\Theta_k,\Phi_k)\Big),\end{aligned} \tag{2.49}$$

where j_0 is the $0th$ order Spherical Bessel Function.

Finally, we can write down the full expression for the window function:

$$W(\vec{k}) = \int \frac{d\hat{k}}{4\pi}\left|\frac{ab}{c^2}\int dR\, R^2 U(R|M)\, 4\pi j_0\Big(kRf(\Theta_k,\Phi_k)\Big)\right|^2. \tag{2.50}$$

We have successfully simplified the $1h$ term by integrating out Φ and Θ, bringing the whole term down to a seven-dimensional integral, with the following integration variables: one halo mass, two axis ratios,

two k-angles and one radial coordinate, whose integral is squared, so effectively that part counts as a two-dimensional integral by itself.

Now, for the $2h$ term, since we already said that we will approximate the halo-halo power spectrum with the linear power spectrum, we can immediately see that it reduces into this form:

$$P^{2h}(\vec{k}) = \frac{1}{\widetilde{\rho}^2}\left[\int dM\, d\mathscr{E}\, d\vec{a}\, n(M)\, b(M)\, M\, p(\vec{a}|M)\, p(\mathscr{E})\, U(\vec{k}|M)\right]^2 P_L(\vec{k})$$
$$= \frac{1}{\widetilde{\rho}^2}\left[\int dM\, d\vec{a}\, n(M)\, b(M)\, M\, p(\vec{a}|M) \int d\hat{k}\frac{ab}{c^2}\int dR\, R^2\, U(R|M)\, j_0\Big(kRf(\Theta_k,\Phi_k)\Big)\right]^2 P_L(\vec{k}), \quad (2.51)$$

where in the second line, we again substitute the integral over orientations with eq. (2.41), we explicitly write down the Fourier transformation of the density profile and we borrow the results of eq. (2.49) to integrate out the angular parts.

Notice how the $2h$ integral, becomes a multiplication of two identical integrals, because of the approximation we chose to make; namely that the halo-halo power spectrum is the linear power spectrum multiplied by two biases, one for each halo. This would not have been the case if we adopted a more complicated halo-halo power spectrum, but as mentioned back in "the Anisotropic Halo-Halo correlation" subsection, such additional terms contribute very little to the total power spectrum, and therefore we justify using the linear approximation based on that.

Chapter 3

Intrinsic Alignments and Halo Models

In this Chapter, we delve into the details of how to construct the power spectra of intrinsic-intrinsic correlations (II), and matter-intrinsic, or density-intrinsic, (δI) correlations that contribute to the total observed shear two-point function which we discussed back in Chapter 1. We will of course use the isotropic halo model to reproduce results similar to those of Schneider & Bridle [10] who were the first to introduce the halo model in intrinsic alignment (IA) modelling. Then we will generalize all this by making our halos ellipsoidal. Thus, we will calculate these power spectra using the anisotropic halo model.

3.1 The HOD model

The halo occupation distribution model, or HOD, is a model in which the necessary tools to start calculating correlations for galaxy clustering are introduced. In the previous Chapter, we only considered correlations of the matter field, as an example on how to set up the isotropic and anistropic halo models. But the halo model is more versatile, so it is useful to introduce more notions like the number of galaxies inside a halo, so that we can write down expressions for galaxy clustering correlations or even IA correlations. The HOD model is extensively discussed in [23][24][25].

The leading slogan here is that the galactic content of our dark matter halos can be divided into central and satellite galaxies. The centrals, as the name suggests, lie at the center of the halo while satelites are distributed according to a density profile $U_s(r|M)$. It is usually assumed that this distribution is an NFW-like distribution, just like in the case of matter.

Now, the number of galaxies contained inside the halo, can be written as functions of the halo mass as follows [24]:

$$\begin{aligned} N_c(M) &= \frac{1}{2}\left[1+\mathrm{erf}\left(\frac{\log(M/M_{min})}{\sigma_{\log M}}\right)\right] \\ N_s(M) &= \Theta(M-M_0)\left(\frac{M-M_0}{M_1'}\right)^{\alpha}, \end{aligned} \tag{3.1}$$

where N_c and N_s are assumed to follow Bernoulli and Poisson distributions respectively, and all other parameters besides the halo mass M, are free parameters which we chose from tables in our references (CCL already does this for us).

Another relevant quantity is the mean number density of galaxies, which will be:

$$\widetilde{n}_g = \int dM\, n(M) N_c(M)(1+N_s(M)). \tag{3.2}$$

3.2 Centrals and Satelites in IA Halo Modelling

As previously mentioned, Schneider & Bridle [10] were the first to use the halo model in the context of IA modelling. In order to that, they used the HOD model. Again, the galaxies are divided into centrals and satellites. The centrals' contribution to the total power spectrum follows the linear alignment model. Hence when trying to model halos for the purpose of IA, we only consider building the contribution of satellites, which follow a distribution and so it makes sense to only choose satelites for halo modelling.

3.2.1 Satellite Contributions

In order to start constructing the satellite power spectra when considering alignment, we ought to start from the beginning, just like how we did with the matter correlations when we started adopted the ansatz that the total density is the sum of halo densities of mass M. Instead of the density, we ought to start from the complex intrinsic shear:

$$\gamma^I(\vec{r}) = |\gamma^I| e^{2i\phi}, \tag{3.3}$$

where $|\gamma^I|$ is called the projected intrinsic shear and ϕ is the azimuthial angle which runs around the line of sight. The projected intrinsic shear oughts to be modelled. In the simplest case, one can say that galaxies look like sticks, with some fixed length $\bar{\gamma}$, and thus the projection onto the sky becomes:

$$|\gamma^I(\theta)| = \bar{\gamma} \sin\theta \tag{3.4}$$

where θ is the polar angle of the galaxy's position from the line of sight. This is called the stick model. In Fortuna et. al [26], they used another model for the projected intrinsic shear, by making the intrinsic shear a function of radius as well:

$$|\gamma^I(r,\theta)| = a_{1h} \left(\frac{r \sin\theta}{r_{200}} \right)^b \tag{3.5}$$

where a_{1h} is a constant and $b = -2$.

How does one combine the complex intrinsic shear from eq. (3.3) with the halo model? Simply multiply it with the normalized density profile used for a halo of mass M:

$$\widetilde{\gamma}^I(\vec{r}, M) = \gamma^I(\vec{r}) U(\vec{r}|M_i). \tag{3.6}$$

The above quantity is named density-weighted intrinsic shear/ellipticity. To obtain the total intrinsic ellipticity field, one must sum over all satellite galaxy over all halos; effectively we must sum over all the masses M_i, where the index i refers to the halo , $\vec{r}_i$ is the i^{th} halos center, and $N_{s,i}$ is the number of satellites contained in the i^{th} halo. We also choose to normalize it with the galaxy number density:

$$\widetilde{\gamma}^I(\vec{r}) = \frac{1}{n_s} \sum_i \gamma^I(\vec{r} - \vec{r}_i)\, N_{s,i}\, U(\vec{r} - \vec{r}_i|M), \tag{3.7}$$

where the ellipticity field is now only a function of position in space. The above can also be written in integral form just like we did with the matter density:

$$\widetilde{\gamma}^I(\vec{r}) = \int d^3r' dm \sum_i \delta^{(3)}(\vec{r}' - \vec{r}_i) \delta(M' - M_i) \frac{N_s(M')}{n_s^2} \widetilde{\gamma}^I(\vec{r} - \vec{r}')\ U(\vec{r} - \vec{r}'|M') \tag{3.8}$$

3.3 Constructing the Isotropic Halo Model for IAs

Now that we have an expression for the ellipticity field of the halos, we can start constructing correlations. It is good to note that, just like [19] mentions, one can take many correlations among density fluctuations,

centrals and satellites, but not all of them are very prominent contributions to the total IA correlation. As Schneider & Bridle [10] showed, of all the correlations contributing to the total IA correlation, the combinations which contribute to the total power spectrum are:

- the 1h density-satellite intrinsic (δI),
- the 1h satellite-satellite intrinsic (II),
- the 2h density-satellite intrinsic (δI),
- the 2h density-central intrinsic (δC),
- the 2h satellite-satellite intrinsic (II),
- the 2h satellite-central intrinsic (IC),
- the 2h central-central intrinsic (CC).

As mentioned at the beginning of section (3.2), we do not consider centrals in the halo model. Which means that the central contributions we will consider, are partially taken from the linear model. We will make an effort to write $1h$ and $2h$ power spectra, using the halo model, for contributions that contain at least a satellite. For centrals, we will adopt the expressions used in [10].

Following a procedure analogous to what we did for matter field power spectra, we can now also write down density-satellite and satellite-satellite correlations or power spectra. For the centrals we do not use the halo model, we just adopt the linear alignment expressions. The quick way to derive the halo-model expressions, is to take the density power spectra in eq. (2.22) and swap out some expressions to substitute in others. Now, we will not have a ($P_{\delta\delta}$) contribution but we will have either a ($P_{\delta I}$) or a (P_{II}) contribution (P_{xI} where x is either δ or I). For each δ in $P_{\delta\delta}$ swapped out for an I, we swap out (from $P_{\delta\delta}$) a mass for a number of satellites, a matter density for a satellite number density, and a normalized density profile for the norm of the density-weighted ellipticity (in real-space for correlations, in k-space for power spectra). We again prefer to focus on only writing down the power spectra again, to avoid convolutions that appear in the real-space expressions of the correlations. Hence the new power spectra will look like this:

$$
\begin{aligned}
P^{s,1h}_{\delta I}(\vec{k}) &= \int dM\, n(M) \frac{M}{\widetilde{\rho}} \frac{N_s(M)}{n_s} |\gamma^I(\vec{k}|M)| U(\vec{k}|M) \\
P^{s,2h}_{\delta I}(\vec{k}) &= \int dM_1\, n(M_1) \frac{M_1}{\widetilde{\rho}} U(\vec{k}|M_1) \int dM_2\, n(M_2) \frac{N_s(M_2)}{n_s} |\gamma^I(\vec{k}|M_2)| P_{hh}(\vec{k}|M_1, M_2) \\
P^{s,1h}_{II}(\vec{k}) &= \int dM\, n(M) \left(\frac{N_s(M)}{n_s} \right)^2 |\gamma^I(\vec{k}|M)|^2 \\
P^{s,2h}_{II}(\vec{k}) &= \int dM_1\, n(M_1) \frac{N_s(M_1)}{n_s} |\gamma^I(\vec{k}|M_1)| \int dM_2\, n(M_2) \frac{N_s(M_2)}{n_s} |\gamma^I(\vec{k}|M_2)| P_{hh}(\vec{k}|M_1, M_2) \\
P^{2h}_{IC}(\vec{k}) &= \frac{C_1 \widetilde{\rho}}{D} P_L(k) \int dM n(M) \frac{N_s(M)}{n_s} b(M) |\gamma^I(\vec{k}|M)| \\
P^{2h}_{\delta C}(\vec{k}) &= \frac{C_1 \widetilde{\rho}}{D} P_L(k) \\
P^{2h}_{CC} &= \frac{C_1 \widetilde{\rho}}{D} P_L(k) \int \frac{d^3k}{(2\pi)^3} \Big[f_E(\vec{k}_1) + f_E(\vec{k} - \vec{k}_1) \Big] f_E(\vec{k}_1) P_L(|\vec{k}_1|) P_L(|\vec{k} - \vec{k}_1|).
\end{aligned}
\tag{3.9}
$$

When the superscript reads s, this denotes a satellite contribution to the power spectra with subscripts xI. When the subscript reads xC, that is a central contribution .

It is now worth to elaborate on how to take the Fourier transformation of the density-weighted ellipticity, present in the satellite power spectra, because it is slightly more technical to obtain than the Fourier of the density profile in the case of the matter power spectra we were dealing with in the previous Chapter.

3.3.1 The Fourier Transformation of the Complex Ellipticity

The Fourier of the density-weighted ellipticity is the following:

$$\begin{aligned}\gamma^I(\vec{k}|M) &= \int d^3r\, \gamma^I(\vec{r},M)\, e^{i\vec{k}\cdot\vec{r}} \\ &= \int d^3r\, \gamma^I(r,\theta)\, U(r|M)\, e^{2i\phi}\, e^{i\vec{k}\cdot\vec{r}}\end{aligned} \tag{3.10}$$

Back in Chapter 2, we discussed how the Fourier transformation of the density profile reduced to a function that depends only on the magnitude of $\vec{k}$. We also mentioned that in the case of alignments, this will not be the case, and now it is time to discuss that. In the case of the density Fourier transformation, one could align the axes of the coordinates we are integrating over such that $\vec{k}$ is entirely aligned with the z-axis of the integration. The Fourier transformation remained invariant under change of coordinates and thus, the result only depended on the magnitude of $\vec{k}$. It was also logical to assume that this would be the case, because matter correlations can not possibly depend on how the observer rotates their view.

In the case of alignments, it is logical that the amount of projected alignment observed **must** depend on the how the observer's coordinates are oriented in space. This becomes manifest in eq. (3.10). If one chooses to rotate the integration variables' axes such that the z-axis becomes parallel to $\vec{k}$, the observed projection changes, because it is a function of the angle θ from the line of sight. Therefore, we cannot make this change of variables without affecting the result. This is entirely dependent on the fact that the integrand, in this case the projected intrinsic shear, changes under coordinate transformation. In the matter case, the integrand did not depend on the observer's orientation (hence the symmetry exploited by Smith & Watts [12] in eq. (2.41)). Though, even if it did, in the isotropic case it would not pose a problem to make the observer's and halo axes coincide, because of the spherical symmetry. But in the anisotropic case, there will be a problem that needs to be solved.

Another difficulty in this expression, at least at first glance, is that it is complex, and to find the norm of this one expression, we need to perform two integrals; one for the real part and one for the imaginary. In the case of the isotropic halo model, this won't be much of a hurdle, since there is a way to solve the angular part analytically. In the case of the anisotropic halo model, this will pose a slight problem, because we will have to completely rely on a numerical solution for the angular part.

Following the appendix of Schneider & Bridle [10], we can perform a plane wave expansion:

$$e^{i\vec{k}\cdot\vec{r}} = \sum_{i=0}^{\infty} (i)^l\, (2l+1)\, P_l(\cos\gamma)\, j_l(kr), \tag{3.11}$$

where P_l and j_l are the Legendre polynomials and the spherical Bessel functions of order l, respectively. The Legendre polynomial's argument $\cos\gamma$ depends on some trigonometric function of the difference of the angles of $\vec{k}$ and $\vec{r}$ [26]. By plugging eq. (3.11) in eq. (3.10), we get:

$$\gamma^I(\vec{k}|M) = \sum_{i=0}^{\infty} (i)^l\, (2l+1)\, U_l(k|M)\, f_l(\theta_k, \phi_k, \beta, \eta), \tag{3.12}$$

where f_l is the total result of the angular integrations and U_l is *approximately* the l^{th} multipole of the NFW profile (it is re-scaled by the projected intrinsic shear):

$$U_l(k|M) = \int dr\, r^2 |\gamma^I|(r,\theta)\, U(k|M)\, j_l(kr). \tag{3.13}$$

In the case one uses the stick model, the intrinsic shear becomes a constant value ($|\gamma^I| = 0.2$), and so it can be pulled out from the integral, leaving U_l exactly equal to the multipoles of the NFW profile. Now, one needs to choose how to move from here by choosing a halo model. In the isotropic halo model, f_l has an analytical solution, whereas in the anisotropic case, as mentioned before, the solution must be obtained numerically.

We see that the Fourier transformation of the density-weighted ellipticity, unlike the Fourier of the density profile in the matter case, is quite tough to tackle, especially in the anisotropic case. There is but one silver lining; it turns out that whether we are in the isotropic or in the anisotropic case, the terms that belong to $l = 0$ or $l =$odd, evaluate to 0, because of the ϕ integral inside f_l. Therefore, the only contributions come from $l = 2,4,6...$, and the result is entirely real. The non-zero multipoles are shown in Figure (3.1). This makes it a lot easier to obtain its norm, and we can approximate the result by stopping at any l which we desire.

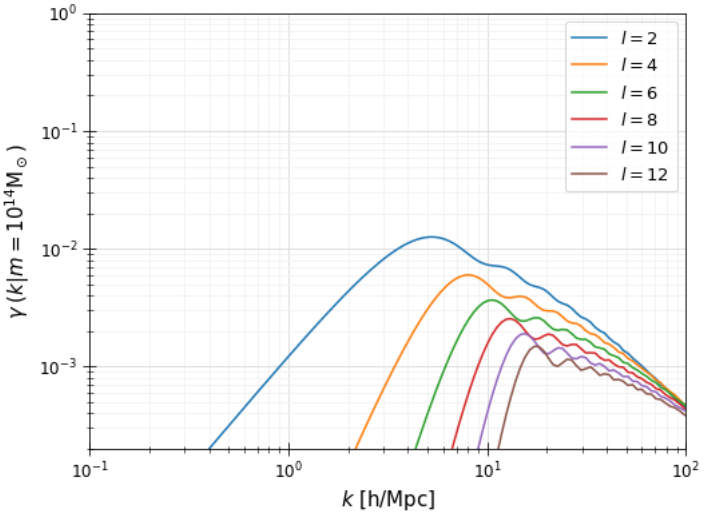

FIGURE 3.1: Multipoles of the Fourier space density-weighted intrinsic shear. The higher multipoles are largely suppressed, and the sum in eq. (3.12) converges quickly.

It is worth repeating, that the result will now depend on the direction of $\vec{k}$, and not just its magnitude, and that dependence rests with f_l. We can notice that the angular part does not alter the shape of the weighted ellipticity when plotted versus k; it merely re-scales the contributions from the NFW multipoles in the sum.

3.4 Constructing the Anisotropic Halo Model for IAs

Now that we understand the isotropic halo model for IAs, it is time to introduce halo anisotropy; we will again consider ellipsoidal halos which follow the shape distribution of Jing & Suto [11] in eq. (2.32).

By following a procedure analogous to what we did with the anisotropic matter power spectra, we will have to promote the density-weighted ellipticity field to contain information about the shape and orientation

of the halo

$$\widetilde{\gamma}^I(\vec{r}) \longrightarrow \widetilde{\gamma}^I(\vec{r},\vec{a},\mathscr{E}) = \sum_i \frac{N_{s,i}}{n_s}\gamma^I(\vec{r}-\vec{r}_i)U(\vec{r}-\vec{r}_i|M,\vec{a},\mathscr{E}) \tag{3.14}$$

just like we did with the density in eq. (2.24). Additionally, since we are using the ellipsoidal coordinates in eq. (2.25), we will have to re-write the Fourier transformation of the complex intrinsic shear, just like we did with the normalized density in eq. (2.42). This will become:

$$\begin{aligned}\gamma^I(\vec{k}|M,\vec{a},\mathscr{E}) &= \int d^3r\,\gamma^I(\vec{r},M,\vec{a},\mathscr{E})\,e^{i\vec{k}\cdot\vec{r}} \\ &= \int d^3r\,\gamma^I(r,\theta)\,U(r|M,\vec{a},\mathscr{E})\,e^{2i\phi}\,e^{i\vec{k}\cdot\vec{r}} \\ &= \frac{ab}{c^2}\sum_l (i)^l(2l+1)\int dRR^2\,U(r|M,\vec{a},\mathscr{E})\,j_l(kR)\int d\Phi\int d\Theta\,\sin\Theta\,\gamma^I(R,\theta)\,e^{2i\phi}\,P_l(\cos\gamma)\end{aligned} \tag{3.15}$$

Notice how the Fourier transform is not just a result of just replacing the old variables with the new ones; there is the expected Jacobian ab/c^2 but, notice how we did not change the angles θ and ϕ into Θ and Φ respectively. The reason is slightly technical. In order to be able to to keep writing an NFW-like profile, using the continuity model we described before introducing the first anisotropic power spectrum in this manuscript, the integration axes should be aligned with the principal axes of the halo. In the case of the isotropic halo, this can always happen trivially because of the spherical symmetry. In the case of the anisotropic one ought to tread more carefully. For the matter power spectra it was still a valid move to

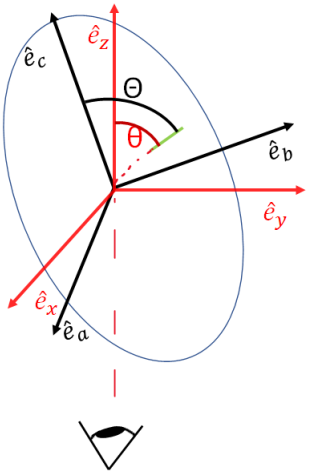

FIGURE 3.2: Pictorial representation of how the observer looks at a galaxy (green stick) at an angle θ from their line of sight. In order to preserve the projected ellipticity, θ should be expressed as a function of Θ and Φ, by relating the two frames (halo and observer frames) through Euler angles.

rotate the integration variables' axes to align with the principal axes of the halo, because we knew what the integrand becomes in that case. But now, we have an integrand that contains a shear projected onto the sky, and that is not invariant under such a rotation. This means that in order to keep the integrand invariant, we should write the angles θ and ϕ (which are measured with respect to the line of sight) as functions of Θ and Φ (which are measured with respect to the major axis of the halo), and not just directly replace the small angles with the big ones. We should, of course, also write the position vector as a function of the new ellipsoidal coordinates, just like we did in the matter case.

To find how θ and ϕ depend on Θ and Φ, one can relate them via a rotation using the Euler angles that connect the observer and the halo frames of reference (as seen in Figure (3.2)). One could have guessed it from earlier, since in the anisotropic case we have degrees of freedom for orientation; the Euler angles.

Also, because now our integrand will contain Euler angles, we cannot impose the symmetry from eq. (2.41) when integrating over orientations. We use the rotation matrix $\mathscr{R}$ used by [19].

A unit vector in the halo's frame of reference is a rotated unit vector from the observer's frame of reference:

$$\hat{e}_{halo}(\Theta,\Phi) = \mathscr{R}(\alpha,\beta,\gamma)\,\hat{e}_{obs}(\theta,\phi). \tag{3.16}$$

To obtain what we want, we need to invert the rotation matrix and multiply it with the halo-unit vector. Remember that to invert a rotation matrix is equivalent to transposing it:

$$\hat{e}_{observer}(\theta,\phi) = \mathscr{R}^T(\alpha,\beta,\gamma)\,\hat{e}_{halo}(\Theta,\Phi). \tag{3.17}$$

We already know how do θ and ϕ depend on the observer's unit vector components:

$$\begin{aligned}\theta &= \arcsin\left(\sqrt{\hat{e}^2_{obs1}+\hat{e}^2_{obs2}}\right)\\ \phi &= \arccos\left(\frac{\hat{e}_{obs1}}{\sqrt{\hat{e}^2_{obs1}+\hat{e}^2_{obs2}}}\right),\end{aligned} \tag{3.18}$$

and now by using eq. (3.17), we can obtain θ and ϕ by substituting in $\hat{e}_{obs1}$ and $\hat{e}_{obs2}$ with whatever they are equal to in terms of Θ, Φ and $\mathscr{E}$ (namely α, β and γ).

Eq. (3.15) then becomes:

$$\gamma^I(\vec{k}|M,\vec{a},\mathscr{E}) = \frac{ab}{c^2}\sum_l (i)^l(2l+1)\,U_l(r|M,\vec{a},\mathscr{E}) \underbrace{\int d\Phi \int d\Theta \sin\Theta\,\gamma^I[R,\theta(\Theta,\Phi,\mathscr{E})]\,e^{2i\phi(\Theta,\phi,\mathscr{E})}\,P_l(\cos\gamma)}_{f_l(\Theta,\Phi,\mathscr{E})}, \tag{3.19}$$

and thus, we obtain something similar to eq. (3.12) (or exactly equal depending on whether you keep the ab/c^2 in or out of U_l), but in this case, f_l cannot be obtained analytically, as already mentioned when we introduced eq. (3.12).

Nevertheless, we can now write down expressions for the $1h$ and $2h$ density-intrinsic and intrinsic-intrinsic power spectra. We simply generalize the expressions in eq. (3.9) into the anisotropic model, the way we did with the matter power spectra in the previous Chapter; namely we promote the mass function $n(M)$ just like eq. (2.30) suggests, and we integrate over shapes and orientations. The central contributions remain the same as before, since they do not have a halo model analogue. Only the density and satellite contributions

change with the model:

$$P_{\delta I}^{s,1h}(\vec{k}) = \int dM\, d\vec{a}\, n(M) p(\vec{a}|M) \frac{M}{\widetilde{\rho}} \frac{N_s(M)}{n_s} \int d\mathscr{E}\, p(\mathscr{E}) |\gamma^I(\vec{k}|M,\vec{a},\mathscr{E})| U(\vec{k}|M,\vec{a},\mathscr{E})$$

$$P_{\delta I}^{s,2h}(\vec{k}) = \int dM_1\, d\vec{a}_1 p(\vec{a}_1|M_1)\, n(M_1) \frac{M_1}{\widetilde{\rho}} \int d\mathscr{E}_1 p(\mathscr{E}_1) U(\vec{k}|M_1,\vec{a}_1,\mathscr{E}_1) \times$$

$$\times \int dM_2\, d\vec{a}_2 p(\vec{a}_2|M_2)\, n(M_2) \frac{N_s(M_2)}{n_s} \int d\mathscr{E}_2 p(\mathscr{E}_2) |\gamma^I(\vec{k}|M_2,\vec{a}_2,\mathscr{E}_2)| P_{hh}(\vec{k}|M_1,M_2)$$

$$P_{II}^{s,1h}(\vec{k}) = \int dM d\vec{a} p(\vec{a}|M)\, n(M) \left(\frac{N_s(M)}{n_s}\right)^2 \int d\mathscr{E}\, p(\mathscr{E}) |\gamma^I(\vec{k}|M)|^2$$

$$P_{II}^{s,2h}(\vec{k}) = \int dM_1\, d\vec{a}_1 p(\vec{a}_1|M_1)\, n(M_1) \frac{N_s(M_1)}{n_s} \int d\mathscr{E}_1 p(\mathscr{E})_1 |\gamma^I(\vec{k}|M_1,\vec{a}_1,\mathscr{E}_1) \times$$

$$\times \int dM_2\, d\vec{a}_2 p(\vec{a}_2|M_2)\, n(M_2) \frac{N_s(M_2)}{n_s} \int d\mathscr{E}_2 p(\mathscr{E})_2 |\gamma^I(\vec{k}|M_2,\vec{a}_2,\mathscr{E}_2)| P_{hh}(\vec{k}|M_1,M_2)$$

$$P_{IC}^{2h}(\vec{k}) = \frac{C_1\widetilde{\rho}}{D} P_L(k) \int dM d\vec{a}\, n(M) p(\vec{a}|M) \frac{N_s(m)}{n_s} \int d\mathscr{E}\, p(\mathscr{E}) |\gamma^I(\vec{k}|M,\vec{a},\mathscr{E})|$$

$$P_{\delta C}^{2h}(\vec{k}) = \frac{C_1\widetilde{\rho}}{D} P_L(k)$$

$$P_{CC}^{2h}(\vec{k}) = \frac{C_1\widetilde{\rho}}{D} P_L(k) \int \frac{d^3k}{(2\pi)^3} \Big[f_E(\vec{k}_1) + f_E(\vec{k}-\vec{k}_1) \Big] f_E(\vec{k}_1) P_L(|\vec{k}_1|) P_L(|\vec{k}-\vec{k}_1|) \tag{3.20}$$

where every term in these integrals is known; the terms concerning the matter contribution in the power spectra can be taken from the previous Chapter under the anisotropic matter power spectra section, and all terms concerning the satellite galaxy contributions for IA can be taken from all the expressions we derived in this subsection. The central contributions remain as they were, except in the *IC* case where the satellite part must be modelled in the anisotropic model.

We have now constructed all the power spectra contributing to the total observed shear correlation, and we have made as many simplifications as we could by substituting in all the analytical results we had. All that remains is to implement a method of numerically calculating all these. We specifically used the Python library "Vegas" [13], which performs Monte Carlo integration, and seems rather suitable for such high-dimensional integrals.

Chapter 4

Results and Discussion

Now that we have got all the theory and formalism down, we are ready to show our predictions. We will assess the success of our modelling and methodology, by comparing with the literature (wherever possible) and by also comparing with what we expected to obtain.

4.1 Matter Power Spectrum Results

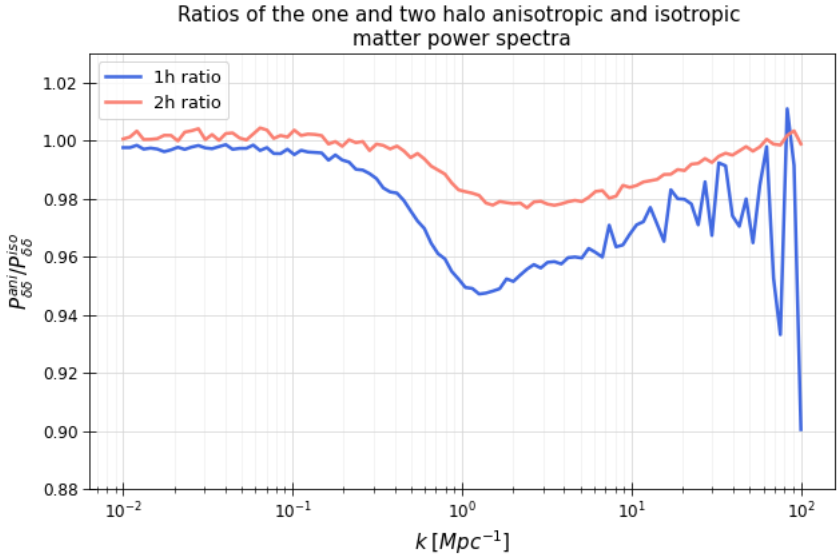

FIGURE 4.1: Ratios of the $1h$ and $2h$ anisotropic and isotropic matter power spectra.

In Figure (4.1), we can see the ratios between the anisotropic and isotropic matter power spectra (the blue one is the ratio of the $1h$ terms whereas the red is for the $2h$ terms). As we can observe, the ratio goes at 1, for small k (large scale in real space), and is fairly constant up until the middle values of k (mid scales in real space). This behavior is expected, since when an observer looks from very far away, the shape and orientation of the halo will not contribute much to the behavior of the power spectrum. This means that whether the halo model is isotropic and anisotropic, they look the same from far away. One can also approximate the anisotropic expressions from Chapter 2 in the limit where k becomes small, to check that they would obtain the equivalent isotropic expressions. Then at the middle to small scales, we see that the anisotrpic contributions are being suppressed. This has been studied before by [12], and the fact that we are reproducing the same results means that we have implemented our formalism successfully. This was an important sanity check, before we moved on to calculate the intrinsic alignment related power spectra, which are more difficult to work with. The above results were produced within an hour, with Monte Carlo integration by use of the Vegas library in Python as we mentioned before, with 10^4 evaluations for the isotropic power spectra and 10^5 for the anisotropic power spectra at each k. The calculation was done in a reasonable time, with reasonable accuracy.

4.2 Intrinsic Alignment Power Spectrum Results

4.2.1 Matter-Intrinsic Contributions

Moving on, for the intrinsic alignment power spectra, we have matter-intrinsic contribution, and intrinsic-intrinsic contributions. Let us first look at the matter-intrinsic ones.

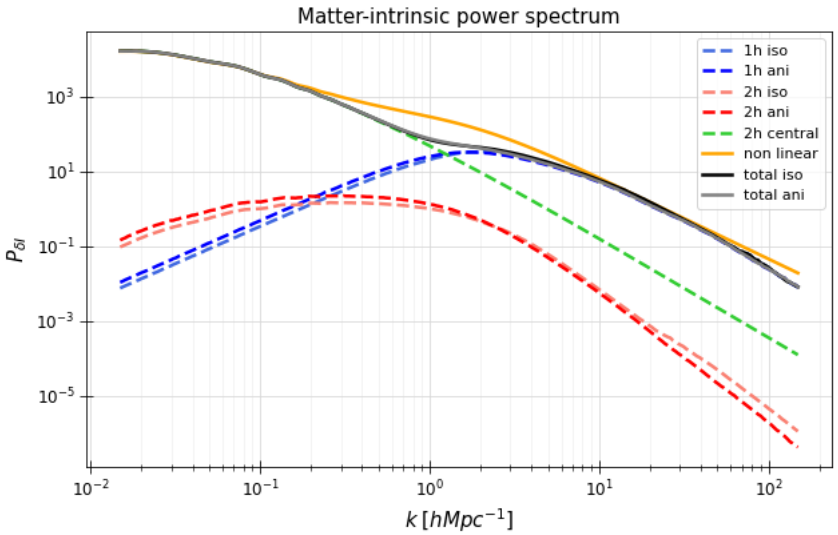

FIGURE 4.2: All the dashed lines are isotropic and anisotropic $1h$ and $2h$ contributions to the total isotropic and anisotropic matter-intrinsic power spectra. The non-linear matter-intrinsic power spectrum is also shown for comparison, as approximated by eq. (14) in [10] or by [17] who were the first to create a linear alignment model, by substituting the non-linear matter power spectrum instead of the linear. This approximation gives a fiducial power spectrum as called by [27].

As seen in Figure (4.2), all the contributions to the total power spectra, whether $1h$ or $2h$, isotropic or anisotropic, were plotted together with the total isotropic and anisotropic power spectra and the so called "fiducial" non-linear matter-intrinsic power spectrum [27], for comparison. The name "fiducial" refers to the power spectrum being empirical and not actually derived. The validity of our halo terms' behavior can be related to the equivalent plot in Fig. (4) in Schneider & Bridle [10]. They were the first to introduce halo modelling for intrinsic alignments, and although they calculated their results at a different redshift than ours, we can see a similarity in the behavior of our isotropic terms, and fiducial non-linear power spectrum. Of course, we went a step further and calculated this for an anisotropic halo model as well. The fact that our isotropic terms look similar to previous work, gives us more confidence in our anisotropic results. Now, if we only focus on the isotropic terms and their respective anisotropic terms, we can observe some slight deviations, but as expected not very large ones.

To examine their relation in more detail, we can also look at Figure (4.3), where we have plotted the ratios between the $1h$ and $2h$ anisotropic and isotropic power spectra. As expected, at large scales, the ratios of both $1h$ and $2h$ contributions are fairly constant. The argument is the same as before; at large scales, it does not matter whether halos are isotropic or anisotropic regarding the behavior of the power spectra. Though, the fact that the ratio does not go to 1, is something that should be checked. Probably, a small k expansion of the anisotropic terms will show whether they become exactly equal to the isotropic terms, or if they differ by a factor of 1.4-1.6, which pushes the ratios above 1 by exactly that many times. In case this factor can be retrieved by a small k expansion, then we can say that the deviation from the isotropic model is an intrinsic property of the anisotropic model. Such a deviation was not seen in the matter power spectrum, but we do not have a good reason to believe that this should be the case for every other power spectrum. Now, in case this cannot be retrieved by the small k expansion, then someone should check whether the problem

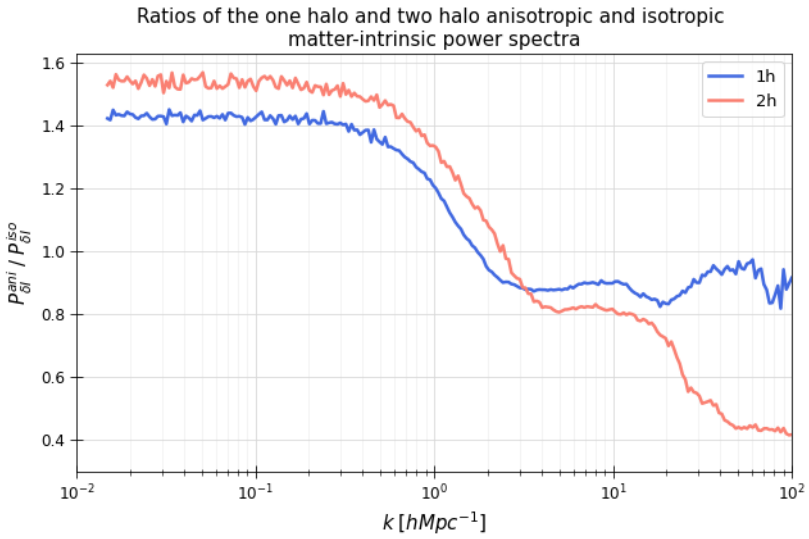

FIGURE 4.3: $1h$ and $2h$ ratios of the anisotropic and isotropic matter-intrinsic power spectra.

lies in the implementation of our expressions e.g a mistake in the code or use of wrong normalization factors.

We have discussed everything regarding the $1h$ and $2h$ terms, so let us now return back to Figure (4.2) and turn our attention to the total power spectra (gray and black lines). At first glance, they seem like they follow the exact same behavior. To further study their relation, we took their ratio as well, as seen in Figure (4.4). As we can see, the total ratios do go to 1 at large scales, which is expected since both are dominated

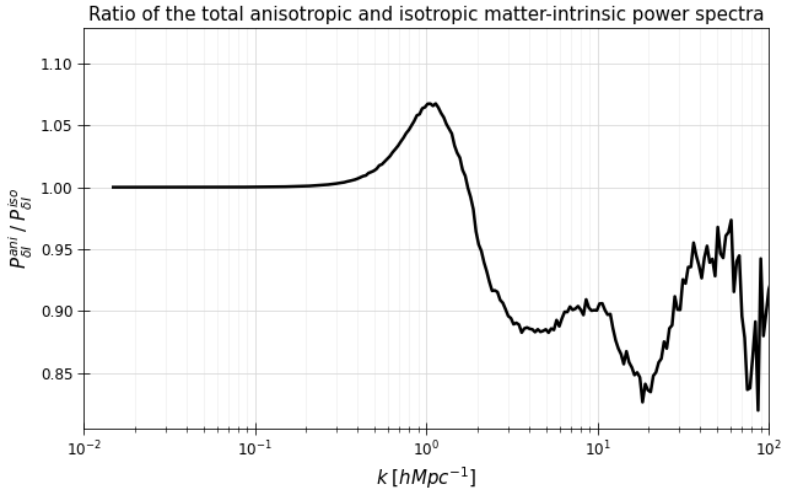

FIGURE 4.4: Ratio of the total anisotropic and total isotropic matter-intrinsic power spectra.

by the central contribution (green curve in Figure (4.2)). But, at the middle scales we can observe that the anisotropic power spectrum tends to spike upwards. This bump is also present in the fiducial non-linear power spectrum. This shows that the anisotropic power spectrum is capturing some of the non-linear effects, but of course the bump occurring there is not comparable to that of the fiducial's. Besides, the fiducial power spectrum is not actually what one should be comparing with. That is because it is an empirical expression, not the underlying truth. It is better to compare with observations such as those of [28] and some more recent observations in [29]. It is worth mentioning, that the anisotropic power spectrum deviates from the isotropic one (which is already a good fit to the observations) by at most 20%, and that is within the error bars of the observations. As a final remark on the anisotropic prediction, the fact that the fiducial and the anisotropic

power spectra have this bump, even if not comparable, shows that the anisotropic model prediction has some merits, given that it is also within the error bars of the observations. Of course, nothing too conclusive can be said unless someone studies the compatibility of the model and the observations in more rigor.

4.2.2 Intrinsic-Intrinsic Contributions

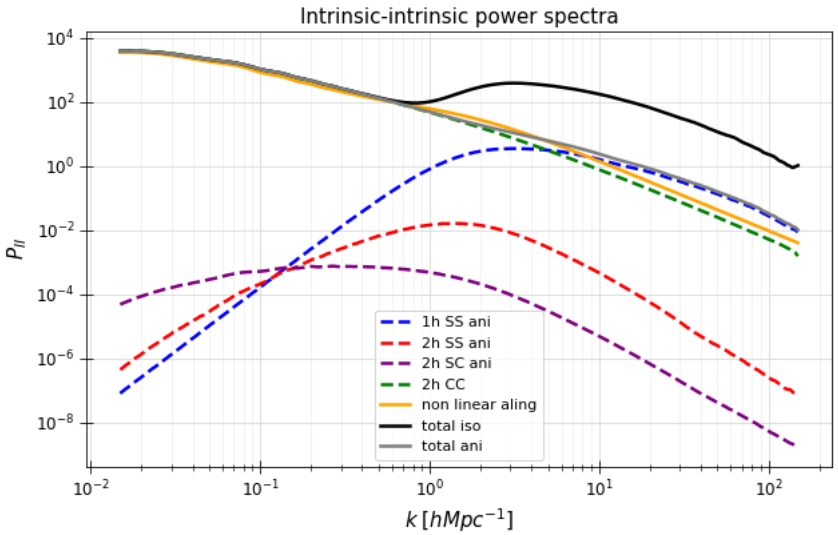

FIGURE 4.5: All the dashed lines are anisotropic $1h$ and $2h$ contributions to the total anisotropic intrinsic-intrinsic power spectra. The non-linear matter-intrinsic power spectrum is also shown for comparison, as approximated by eq. (1.16) or by [17] who were the first to create a linear alignment model, but by substituting the non-linear matter power spectrum instead of the linear. This approximation again gives a fiducial power spectrum as called by [27], but for the intrinsic-intrinsic case.

It is now time to start looking at the intrinsic-intrinsic contributions. In Figure (4.5), we plotted all the anisotropic contributions to the total power spectrum, the total anisotropic power spectrum, the total isotropic power spectrum and the fiducial non-linear intrinsic-intrinsic power spectrum. Let us first talk about the difference between the $1h$ and $2h$ isotropic and anisotropic contributions. The isotropic contributions are not plotted, because the plot would become too cluttered. So let us promptly jump to the ratio of the two models, in Figure (4.6). Similarly to the matter-intrinsic case, the ratio does not go to 1, but it is fairly constant,

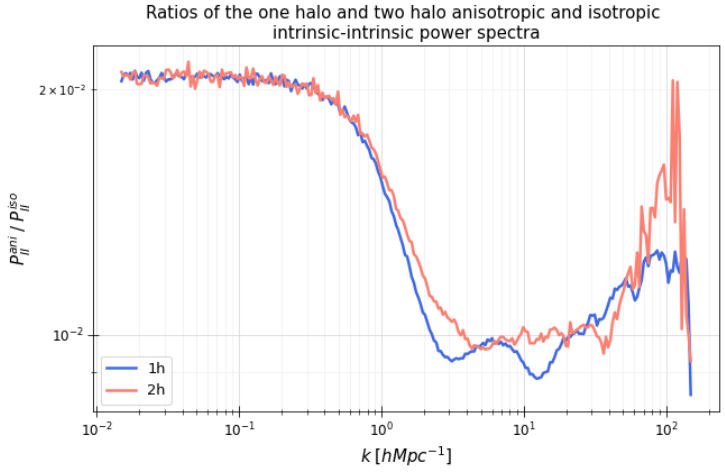

FIGURE 4.6: Ratios of the 1h and 2h anisotropic and isotropic intrinsic-intrinsicc contributions.

as expected, at large scales. Again, one must check whether the anisotropic model intrinsically does not converge to the isotropic model at the limit where k is small, by performing a small k expansion on the anisotropic results. If it does converge to the isotropic expression, then the problem may lie in our implementation. We have meticulously checked several times but we could not identify any such problem. Even if the ratio does not go to 1, we can still see that it is fairly constant, a common and rather expected behavior judging from the previous ratios we examined. Apparently, the anisotropic intrinsic-intrinsic contribution is also suppressed, by 50% in the mid to low scales.

To further comment on that, let us turn our attention back to Figure (4.5), specifically to the total power spectra. We can immediately observe that in the large-scale they are all equal. But at the mid to low scales, the anisotropic power spectrum fits extremely well the fiducial power spectrum, compared to the isotropic power spectrum which largely over-determines the "true" value (the fiducial is of course not the true value, but for the sake of argument we use the word true in quotes). Similarly to the matter-intrinsic results, we cannot rush into the conclusion that the anisotropic model does a very good job at capturing the non-linearities of the system (even if in this case, the anisotropic model is a way better fit than the isotropic, unlike in the matter-intrinsic case where they were very similar fits). The reason is again that, the fiducial non-linear power spectrum is not the underlying truth, but rather an empirical expression. Sadly, not much can be determined from observations, because the observations regarding intrinsic alignments are rather poor, as reported in [30]. But, there are some simulation results like in [31] and [32], which ought to give something better to compare to. It is worth mentioning, as a final remark, that even though we do not have good observational constraints for the total intrinsic-intrinsic power spectrum, the fact that the anisotropic model fits the fiducial non-linear model so much better than the isotropic is certainly a very interesting prediction.

Chapter 5

Conclusion

A the beginning of this manuscript, we introduced the branch of Cosmology, in a brief yet concise manner. We mentioned some of the probes that interest cosmologists in their journey to find out more about the nature of dark matter and dark energy. One of those probes is weak lensing. Lensing effects can tell us a lot about the distribution of matter and energy around the Universe. One powerful way to study lensing (or fluctuations of fields) is in a statistical manner: namely through correlation functions, or their Fourier analogue, their power spectrum. These power spectra, encapsulate the initial conditions of our Universe, which we believe to be Gaussian, and that is why it suffices to only consider two-point correlations for our study. Now the correlation between two observed shears, is not the real correlation of the cosmic shear. It is "contaminated" by correlations between intrinsic alignments and between matter and intrinsic alignments. In order to study the cosmic shear, we should know which part of the data is contamination and which is real. In order to model alignment correlations and power spectra we use the halo model. The first to have done this were Schneider & Bridle in [10], by using the isotropic halo model.

Now, remember how we said that the initial conditions of the Universe are Gaussian. As the LSS grows, non-linear procedures occur, due to gravity, and therefore non-Gaussianities enter our correlations, which may lead to anisotropies at smaller scales. In the linear model, the various correlations and power spectra are accurate at large scale, where the non-linear effects are not very prominent. But as we go to smaller and smaller scales, the linear model fails to determine what the power spectra should be, and that is why people have tried using the halo model, to produce correction terms for the linear model. But as we said, due to non-Gaussianities growing, we expect some anisotropy at smaller scales, and that is why we extend the halo model from the isotropic to the anisotropic halo model. In the anisotropic halo model, all matter in the Universe is still partitioned within halos, but our halos are now ellipsoidal; they have various shapes and orientations.

We first checked whether we could reproduce results from previous work, by using the anisotropic model. Namely we tried reproducing the matter power spectrum. We successfully did so, and then we tried reproducing the isotropic halo model for intrinsic alignments. Once we also got reasonable predictions, that were in line with previous work, we tried predicting the exact same power spectra in our own new way; that is to produce intrinsic alignment power spectra using the anisotropic halo model!

We mentioned how one generalizes the analytical isotropic expressions to analytical anisotropic expressions (with all the caveats and difficulties, which were not present in the case of the anisotropic matter power spectrum) and all that remained was to numerically calculate them.

Once calculated, we plotted our results and compared them with fiducial power spectra of alignments, due to lack of better expressions to compare to. We observed that the anisotropic model, both for the matter-intrinsic power spectrum and the intrinsic-intrinsic one, is trying to capture the non-linearity in the smaller scales. We could not give a very conclusive result whether these are truly the correct power spectra, since our point of reference were the fiducial power spectra, which are empirically derived.

That is why these results should not yet be interpreted as the underlying truth. They are predictions to which we gave good reasons as to why we believe them in them. We also gave directions towards one should move to check these predictions. One should be looking at observations for the matter-intrinsic power spectrum whereas for the intrinsic-intrinsic one, there have not been reliable observations yet so we must turn our attention in constraining it through simulations.

We also noted some instances where the model ought to be checked. One of those instances was to check whether the anisotropic $1h$ and $2h$ terms intrinsically deviate in magnitude from the isotropic analogues, making their ratio not equal to 1 at large scales. Another possible improvement would be, to use a better numerical method for the computation of the power spectra. We used the Vegas library to perform Monte Carlo integration, with 10^5 steps per k for each of our terms (except the isotropic ones where 10^4 steps seemed good enough). We should note that, the intrinsic alignment integrals, especially the anisotropic, are very high-dimensional. This means that even by using Monte Carlo integration with importance sampling, the results may still have rather large error bars. A way to go around this would be to use more steps, but then it would take a considerable amount of time to finish with those calculations. We tried to partially solve those integrals analytically as much as we could, before implementing numerical methods, to reduce their dimensionality. Someone else may be willing to find another trick to lower the dimensionality of those integrals, making them easier to solve numerically. And of course, as a last suggestion and maybe an obvious one, one may implement another method of integration which we have not thought of. Depending on the method, it might yield even more accurate results, in a reasonable amount of time.

Bibliography

1. Dodelson, S. & Schmidt, F. *Modern cosmology* (Academic Press, 2020).
2. Chaisson, E. J. The three eras of cosmic evolution. *World Futures: Journal of General Evolution* **23,** 11–29 (1987).
3. Joachimi, B. *et al.* Galaxy alignments: An overview. *Space Science Reviews* **193,** 1–65 (2015).
4. Blanton, M. R. *et al.* Sloan digital sky survey IV: Mapping the Milky Way, nearby galaxies, and the distant universe. *The Astronomical Journal* **154,** 28 (2017).
5. Colless, M. *et al.* The 2df galaxy redshift survey: spectra and redshifts. *Monthly Notices of the Royal Astronomical Society* **328,** 1039–1063 (2001).
6. De Jong, J. T., Verdoes Kleijn, G. A., Kuijken, K. H. & Valentijn, E. A. The kilo-degree survey. *Experimental Astronomy* **35,** 25–44 (2013).
7. Abbott, T. *et al.* The Dark Energy Survey: more than dark energy–an overview. *Monthly Notices of the Royal Astronomical Society* **460,** 1270–1299 (2016).
8. Cooray, A. & Sheth, R. Halo models of large scale structure. *Physics reports* **372,** 1–129 (2002).
9. Cacciato, M., Lahav, O., van den Bosch, F. C., Hoekstra, H. & Dekel, A. On combining galaxy clustering and weak lensing to unveil galaxy biasing via the halo model. *Monthly Notices of the Royal Astronomical Society* **426,** 566–587 (2012).
10. Schneider, M. D. & Bridle, S. A halo model for intrinsic alignments of galaxy ellipticities. *Monthly Notices of the Royal Astronomical Society* **402,** 2127–2139 (2010).
11. Jing, Y. & Suto, Y. Triaxial modeling of halo density profiles with high-resolution N-body simulations. *The Astrophysical Journal* **574,** 538 (2002).
12. Smith, R. E. & Watts, P. Triaxial haloes, intrinsic alignments and the dark matter power spectrum. *Monthly Notices of the Royal Astronomical Society* **360,** 203–215 (2005).
13. Lepage, G. P. Adaptive multidimensional integration: VEGAS enhanced. *Journal of Computational Physics* **439,** 110386 (2021).
14. Tong, D. Lectures on cosmology. *Cambridge University* (2019).
15. Meerburg, P. D. *et al.* Primordial Non-Gaussianity. *arXiv preprint arXiv:1903.04409* (2019).
16. Chisari, N. E. *et al.* Core cosmology library: Precision cosmological predictions for LSST. *The Astrophysical Journal Supplement Series* **242,** 2 (2019).
17. Hirata, C. M. & Seljak, U. Intrinsic alignment-lensing interference as a contaminant of cosmic shear. *Physical Review D* **70,** 063526 (2004).
18. Harris, C. R. *et al.* Array programming with NumPy. *Nature* **585,** 357–362 (2020).
19. Zwol, B. v. *Anisotropic Haloes and Intrinsic Alignments* MA thesis (2022).
20. Tinker, J. L. *et al.* The large-scale bias of dark matter halos: numerical calibration and model tests. *The Astrophysical Journal* **724,** 878 (2010).

21. Navarro, J. F. *The structure of cold dark matter halos* in *Symposium-international astronomical union* **171** (1996), 255–258.

22. Duffy, A. R., Schaye, J., Kay, S. T. & Dalla Vecchia, C. Dark matter halo concentrations in the Wilkinson Microwave Anisotropy Probe year 5 cosmology. *Monthly Notices of the Royal Astronomical Society: Letters* **390,** L64–L68 (2008).

23. Zheng, Z. *et al.* Theoretical models of the halo occupation distribution: Separating central and satellite galaxies. *The Astrophysical Journal* **633,** 791 (2005).

24. Nicola, A. *et al.* Tomographic galaxy clustering with the Subaru Hyper Suprime-Cam first year public data release. *Journal of Cosmology and Astroparticle Physics* **2020,** 044 (2020).

25. Koukoufilippas, N., Alonso, D., Bilicki, M. & Peacock, J. A. Tomographic measurement of the intergalactic gas pressure through galaxy–tSZ cross-correlations. *Monthly Notices of the Royal Astronomical Society* **491,** 5464–5480 (2020).

26. Fortuna, M. C. *et al.* The halo model as a versatile tool to predict intrinsic alignments. *Monthly Notices of the Royal Astronomical Society* **501,** 2983–3002 (2021).

27. Bridle, S. & King, L. Dark energy constraints from cosmic shear power spectra: impact of intrinsic alignments on photometric redshift requirements. *New Journal of Physics* **9,** 444 (2007).

28. Singh, S., Mandelbaum, R. & More, S. Intrinsic alignments of SDSS-III BOSS LOWZ sample galaxies. *Monthly Notices of the Royal Astronomical Society* **450,** 2195–2216 (2015).

29. Samuroff, S. *et al.* The Dark Energy Survey Year 3 and eBOSS: constraining galaxy intrinsic alignments across luminosity and colour space. *arXiv preprint arXiv:2212.11319* (2022).

30. Blazek, J., McQuinn, M. & Seljak, U. Testing the tidal alignment model of galaxy intrinsic alignment. *Journal of Cosmology and Astroparticle Physics* **2011,** 010 (2011).

31. Samuroff, S., Mandelbaum, R. & Di Matteo, T. Testing the impact of satellite anisotropy on large- and small-scale intrinsic alignments using hydrodynamical simulations. *Monthly Notices of the Royal Astronomical Society* **491,** 5330–5350 (2020).

32. Kurita, T. *et al.* Power spectrum of halo intrinsic alignments in simulations. *Monthly Notices of the Royal Astronomical Society* **501,** 833–852 (2021).